Navarro-Gómez, A.; Bonet Senach, JL. (2019). Improving the seismic behaviour of Reinforced Concrete Moment Resisting Frames by means of SMA bars and Ultra-High Performance Concrete. Engineering Structures. 197:1-20. https://doi.org/10.1016/j.engstruct.2019.109409

IMPROVING THE SEISMIC BEHAVIOUR OF REINFORCED CONCRETE MOMENT RESISTING FRAMES BY MEANS OF SMA BARS AND ULTRA-HIGH PERFORMANCE CONCRETE

A. Navarro-Gómez[1], José L. Bonet[2]

[1] Instituto Universitario de Ciencia y Tecnología del Hormigón (ICITECH), Universitat Politècnica de València, Vera Street unnumbered, Valencia, 46022, Spain
alnagme@upv.es

[2] Instituto Universitario de Ciencia y Tecnología del Hormigón (ICITECH), Universitat Politècnica de València, Vera Street unnumbered, Valencia, 46022, Spain
jlbonet@cst.upv.es

Abstract.

In the design of concrete buildings in seismic zones, ductility is normally used to reduce design efforts and as a form of energy dissipation. This implies structural damage to buildings in the form of interstorey drifts that need to be subsequently repaired or demolished.

Twelve moment resisting frames (MRF) were designed with different geometrical configurations and new materials, and shape memory alloy bars and ultra-high performance concrete were used in the critical zones of the structure to improve their seismic behaviour. MRFs were subjected to a non-linear static pushover analysis and an incremental dynamic analysis to assess their behaviour. To do so, six real accelerograms were selected to study the response of the 12 MRFs, scaled at increasing peak ground acceletation (PGA). The base shear, the building's overall plastic mechanism and the seismic response factors for the different geometrical and material combinations were analysed. The obtained values were compared with ASCE 7-05 and EC-8 proposals.

It was concluded that the combination of shape memory alloys and ultra-high performance concrete allowed the behaviour factor to increase and residual drifts to decrease, which are advantages for both design and seismic behaviour.

Keywords.

Shape memory alloys, ultra-high performance concrete, earthquake engineering, pushover analysis, incremental dynamic analysis, ductility.

Highlights.

- Design MRF with new materials: SMA and UHPC.
- New constitutive models in OpenSees.
- Incremental dynamic analysis for a varied set of ground motions.
- SMA and UHPC reduce residual drifts.
- Calculation of values for the behaviour factor.

1. Introduction.

Damage caused by earthquakes in concrete constructions tends to concentrate in the zones of the joints between several elements, and is due to the crushing of the concrete cover and the large plastic deformations of steel longitudinal reinforcement [1]. This produces large residual deformations in the structure after an earthquake, which means economic loss as reconstruction needs repairing. The use of new materials, such as shape memory alloy reinforcing bars with superelasticity (SMA-SE) and high- or ultra high-performance concrete, in critical zones of structures can help mitigate their damage and, consequently, the economic costs of repair [2].

Shape memory alloys (SMA) are materials capable of recovering deformations of up to 10% after heating or removing the applied load [3]. The ability of SMA to deform under load and to recover their original shape after heating is known as the shape memory effect. If they are able to recover their original shape after loading and load release, this phenomenon at room temperature is known as superelasticity. Currently, there is a tendency to combine these functional SMA properties with the structural properties of other materials [4]. The good hysteretic and oxidation properties of these materials make them ideal for their application with composite materials in anti-seismic construction [5]. Numerous experimental research works are found in the literature that

have assessed the potential of using SMA-SE bars to reinforce structures subject to earthquakes. It has been concluded that their use as reinforcement in column-foundation connections in combination with ECC in the plastic hinge area of an isolated element subjected to lateral loads reduces plastic rotations and the damage undergone by the prototypes reinforced with this material for similar load levels [6]. Other studies have recommended its use in beam-column joints with good results in plastic deformations terms compared to elements built with conventional materials [7]. Considerable reductions in residual deformations have also been obtained when constructing concrete beams reinforced with this type of alloys and subjected to four-point bending tests [8]. Recently, Pereiro et al. [2] presented an experimental numerical study of columns manufactured with high-performance concrete (HPC) and ultra high-performance (UHPC) with NiTi SMA-SE bars located in critical zones, subjected to constant axial force and cyclic lateral load. In these specimens, a residual drift ratio below 0.70% was generally observed for a drop in the maximum lateral load of less than 20%. Minor damage was observed in the critical zone of the column as a result of the high fibre content in concrete. The specimens manufactured with UHPC displayed better overall performance.

The literature contains some recent examples of modelling the behaviour of structures reinforced with SMA bars. Shrestha and Hao [9] analysed the performance of bridge piers reinforced with SMA in simulations with a wide set of earthquakes, and showed minor damage measured in residual deformation terms. Zafar and Andrawes [10] carried out simulations of substituting steel reinforcements in the beam-column and the column-foundation area of 2D frames built with concrete reinforced with GFRP bars and bars made of a composite material consisting of SMA and FRP fibres. The time domain simulations of a set of real accelerograms showed better behaviour in terms of residual drifts for the latter, but with greater deformability. In another study [11], the authors explored the effect of the duration factor, and concluded that SMA-FRP reinforced frames exhibited less vulnerability to aftershocks in terms of accumulating

residual permanent drifts compared to steel-reinforced frames. This shows the importance of the SMA re-centering capability to mitigate the effects of sequential ground motions. Alam et al [12] performed a numerical calibration of an isolated beam-column element reinforced with SMA-SE NiTi, to determine plastic hinge length, and to develop a bond-slip model to take into account the slippage in the mechanical connectors used in the experimental programme. Alam et al. [13] carried out simulations on mid-rise concrete frames reinforced with superelastic SMA bars in the plastic hinge regions, subjected to a set of ground motions. They previously validated the FEM model at element level using the results of a shake table test of a three-storey moment resisting steel RC frame. Later Alam et al. [14] carried out simulations in buildings designed with that element, in which SMA-reinforced concrete was included only in the plastic hinge zone of beams, with columns made of conventional reinforced concrete. They concluded that bigger drift demands were obtained for SMA-reinforced buildings, especially low-rise buildings, as well as lower demands in base shear terms compared to a conventional design made with steel reinforcements. Youssef et al. [15] also simulated different SMA design alternatives to define the locations of SMA bars in typical RC frames to optimise their seismic performance in terms of damage scheme and seismic residual deformations.

UHPC is a concrete type whose compressive strength exceeds 100 MPa that is composed of a cementitious matrix reinforced with steel fibres and high-performance additives to allow it to reach high ductility and to develop strain-hardening behaviour against uniaxial tensile stress [16]. Several authors have performed experimental tests on elements built with UHPC. Takatsu et al. [17] studied the seismic behaviour of UHPC columns, and concluded that steel fibres increase lateral load capacity, and that column strength increases with the fibre volume falling within the studied range. Voo et al. [18] studied the shear behaviour of prestressed beams with no transverse reinforcement. The high volume of fibres in the concrete matrix led to a plastic response. Zohrevand and Mirmiran [19] tested circular-section cantilever columns

manufactured with hybrid concrete of HPFRC and FRC under cyclic loading. Columns showed microcracking with no cover spalling, unlike conventional concrete. The use of UHPC in the plastic hinge area significantly increased both stiffness and resistance, and reduced the amount of longitudinal and confinement reinforcement. Popa et al. [20] experimentally and numerically studied the behaviour of columns manufactured with a UHPC core and a conventional concrete cover under monotonic load. Columns displayed fragile behaviour as compression strength increased. Kamal et al. [21] applied a monotonic load to test simple bending UHPC beams reinforced with two fibre types: steel and polypropylene. The former proved more efficient regardless of the amount by increasing both cracking and ultimate load. Maya et al. [22] tested precast column-beam joints with a new distribution of longitudinal and transverse reinforcement under cyclic loading. They obtained improvements in both element behaviour and the location of damage inside the joint, but pointed out the need to improve ductility and to control the crack opening in the discontinuity section.

Their recentring capacity and energy dissipation make SMA-SE bars an ideal material to improve the behaviour of structures in seismic zones. However, the main obstacle is their high manufacturing cost, especially for those bars with the usual diameters manufactured in the construction industry. Therefore, their strategic use in areas where they are most cost-effective is necessary. For MRF, beam-column joints are designed to be rigid, which results in considerable damage in those zones [10].

The use of SMA in the construction field [23], and the joint use of NiTi SMA bars with HPC or UHPC, are relatively new. Employing these new materials needs to be studied as the simultaneous simulation of the behaviour of hybrid structures manufactured with SMA-SE bars and UHPC under monotonic and cyclic loads is novel. This study comparatively analysed the substitution of conventional materials in these areas. Unlike previous studies, this study included the replacement of not only steel bars with

SMA, but also of the concrete material in the structure's critical regions with HPC materials to overcome the limitations of conventional concrete.

Specifically, this study analysed the seismic behaviour of concrete buildings in which steel bars were substituted in their critical zones for superelastic SMA bars (NiTi SMA-SE). As NiTi SMA-SE bars have a deformation modulus that is 3 to 4-fold less than that of steel, greater displacements in the structure and greater deformability of concrete were expected achieved. For this reason, the convenience of replacing conventional concrete in critical zones with new concrete types that have higher deformation capacity and ductility was verified. A pushover analysis and an incremental dynamic analysis were performed herein to analyse the seismic behaviour in terms of behaviour factors and residual drifts. Finally, the behaviour factor for the analysed buildings was obtained.

2. Designing structural prototypes.

2.1. The RC-MRF prototype.

Two types of reinforced concrete 2D frames were herein studied: one consisted of a single bay and three storeys (3S1B), while the other comprised two bays and six storeys (6S2B). They were used to evaluate the effect that the structure's different geometries could have on seismic behaviour. In both frames, span was 6.5 m and storey height was 3.6 m. These dimensions are representative of regular building structures. An interior building frame was analysed in both cases. The critical zones where the plastic hinges of the column-foundation and the beam-column joint of the first storey can be developed, along with the beam-column joint of the subsequent storeys, were modified by replacing conventional materials with different combinations of materials: conventional concrete (NSC), HPC and UHPC; and by reinforcing materials: steel and SMA-SE. Outside these zones, the structure was made of conventional reinforced concrete. Therefore, 12 different frames were modelled and

each one was identified by the combination of materials used in critical zones (see Tables 1 and 2).

Table 1. Design values and reinforcement arrangement for building 3S1B.

Materials in critical zones	T_1 (s)	V_{bd} (kN)	Beam reinf.	ρ (%)	Column reinf.	ρ (%)
Steel & NSC	0.557	130	6ϕ16	1.79	8ϕ16	2.01
SMA & NSC	0.652	111	5ϕ16	1.49	7ϕ16	1.76
Steel & HPC	0.484	149	5ϕ16	1.49	6ϕ16	1.51
SMA & HPC	0.556	129	4ϕ16	1.19	5ϕ16	1.25
Steel & UHPC	0.478	151	5ϕ16	1.49	7ϕ16	1.78
SMA & UHPC	0.497	145	4ϕ16	1.19	5ϕ16	1.26

Table 2. Design values and reinforcement arrangement for building 6S2B.

Materials in critical zones	T_1 (s)	V_{bd} (kN)	Beam reinf.	ρ (%)	Column reinf.	ρ (%)
Steel & NSC	1.17	243	7ϕ16	2.09	8ϕ16	2.01
SMA & NSC	1.21	206	6ϕ16	1.79	9ϕ16	2.23
Steel & HPC	1.14	272	6ϕ16	1.79	8ϕ16	2.01
SMA & HPC	1.16	262	4ϕ16	1.12	5ϕ16	1.26
Steel & UHPC	1.12	279	4ϕ16	1.12	7ϕ16	1.76
SMA & UHPC	1.15	269	5ϕ16	1.49	8ϕ16	2.01

The aims of substituting these materials in critical zones were to form a mechanism of plastic hinges on the first storey level that isolated the rest of the structure from most seismic effects, and to reduce damage on upper floors by modifying the plastic hinge zones on the beam-column joint, where large plastic rotations tend to concentrate. Checks were made to see if the recentering capacity of SMA helped to reduce residual deformations and to, consequently, cut repair costs. A medium ductility class (DCM) was considered to design the reinforcement of building elements according to EC 8-1 [24]. For this ductility class, the critical zone length for beams equals the beam's depth, and for columns it is the highest value among the column's depth, one sixth of the free height of the support and 450 mm; i.e., 562.5 mm, the equivalent to 1.4-fold the column's depth. Nevertheless, the critical zone length was extended to 1.5-fold the depth in both beams and columns to avoid fragile failure at the interface between the critical zone and the rest of the element as each part was built with different concrete types (UHPC-NSC or HPC-NSC) and distinct types of bars (steel-SMA). During the

design process, checks were also made to see if this length sufficed to avoid fragile failure in the hinge-rest on the element interface., Pereiro-Barceló et al. [25] have been able to experimentally confirm the adequate behaviour of the joint between the critical zone and the rest of the element under cyclic loading. A length equal to 1.5-fold the depth has also been considered by Zafar and Andrawes [10,11]; i.e., the critical zone length was 675 mm for beams and 600 mm for columns. These lengths were considered constant for all the designs to avoid introducing another variable. The position of the modified zones is seen in Figure 1. The rest of the structure was designed with conventional concrete and steel reinforcements. It has been verified that the critical zone length is longer than the plastic hinge length. In the technical literature, no expression is found for calculating the plastic hinge length for the elements manufactured with UHPC or HPC reinforced with SMA bars. Recently, Billah and Alam [26] proposed an equation to calculate the plastic hinge length of SMA-RC bridge piers valid up to 75 MPa. Consequently in the absence of a proposal for UHPC or HPC elements reinforced with SMA rebars, the well-known equation (1) proposed by Paulay and Priestley [27], and recommended by Alam et al. [12] for SMA RC, was used to calculate plastic length:

$$l_p = 0.08 \cdot L + 0.022 \cdot d_{SMA} \cdot \sigma^{M_s} \quad (1)$$

where L is, for beams, the distance from the face of the beam-column joint to the beam's mid-span and, for columns, the distance from the face of the beam-column joint or the column-foundation to half the column height; d_{SMA} is the SMA bar diameter SMA in mm; σ^{M_s} is the austenite-to-martensite starting stress in MPa. Thus the plastic hinge length equals 272 mm for columns and 381 mm for beams. The position of the modified zones is seen in Figure 1. The rest of the structure was designed with conventional concrete and steel reinforcements.

In order to avoid the effect of the dimensions of the structure's elements on dynamic behaviour, all the beams are 0.45 m deep and 0.30 m wide, all the columns were 0.4 m deep and 0.4 m wide.

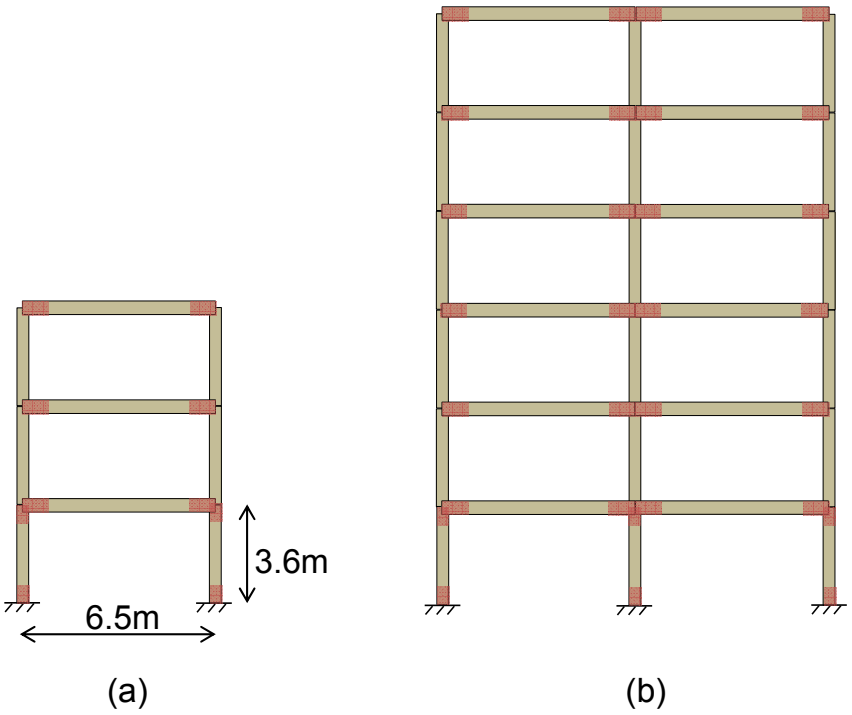

Figure 1. Prototype 2D-reinforced concrete MRF and the position of the modified joints with new materials. a) 3S1B b) 6S2B.

2.2. Design process.

To design the reinforcing of building elements, elastic response spectrum type 1, as recommended in Eurocode 8 [24], was taken as a reference, along with the equivalent lateral force method as described in the same code. The building was considered to be located on ground type B with a basic acceleration of 0.25 g, corresponding to L'Aquila (Italy), and that the building is specially important. In preliminary terms, the default values of the α_u/α_1 ratio, 1.2 and 1.3 respectively, were taken as being valid to calculate frames 3S1B and 6S2B, where α_u is the load factor to design base shear V_{bd} to produce overall instability due to plastic hinge formation, and α_1 is the load factor in the first yield in the structure. A basic q_0 value of the behaviour factor of 3 was chosen,

which corresponds to a medium ductility class for concrete torsionally flexible structural systems. This value is discussed later.

For the design, the characteristics of the materials obtained in previous experimental studies were considered [2]: for NSC, compressive strength f_{co} that equalled 26.5 MPa and Young's modulus E_c that equalled 27500 MPa; for HPC to which steel fibres of 80 kg/m^3 were added, compressive strength f_{co} that equalled 74.8MPa and E_c 35000 MPa; for UHPC to which steel fibres of 150 kg/m^3 were added, compressive strength f_{co} equalled 116.5 MPa and E_c was 46000 MPa. Regarding reinforcing materials, a yield strength of 540 MPa and a Young's modulus of 200000 MPa were considered for the steel rebars; and an direct transformation onset strength of 389 MPa and an austenitic Young's modulus E_A of 64833 MPa were contemplated for the SMA rebars.

For the values of actions, Eurocode 1 was taken as a reference [28]. For the dead load, 3.6 kN/m^2 was taken for the floor slab, 1 kN/m^2 for floor finishes and 3.5 kN/m^2 for the façade. For live loads, 5 kN/m^2 was taken for all the floors and 2.0 kN/m^2 for the top roof. By taking these loads, masses were estimated by tributary areas and the basal design shear was calculated according to the procedure in Eurocode 8. To determine gravitational loads, a combination factor for the live loads of 0.30 was selected. Preliminary reinforcement was adopted to calculate the structure's natural period (T_1) by a modal analysis of the non-linear model. The modal analysis was carried out with the homogenised section of all the elements after applying gravitational loads and before applying the equivalent lateral load. Next the spectral acceleration value was obtained from the design response spectrum, and basal shear V_{bd} was calculated. This design shear force was distributed along the building's height. According to the distribution of the equivalent horizontal seismic forces proposed by Eurocode 8 [24], two different distributions were taken: one uniform distribution and an inverted triangular one that corresponded to the structure's first mode. The most unfavourable distribution was chosen, which was herein the inverted triangular charge for all cases.

Having applied the gravitational loads to the structure, a pushover analysis was performed on the linear elastic equivalent model for both distributions (uniform and inverted triangular) to obtain stresses in critical sections. As the traditional deformation domains were not valid for the SMA reinforcement and the new concrete materials, a non-linear moment-curvature sectional analysis was carried out with the constitutive equations of the materials in OpenSees. The necessary amount of reinforcement was obtained in such a way that the available capacity equalled the design demand. Another requirement that must be fulfilled is the strong column and weak column design principle to avoid plant failures. As this new reinforcement arrangement would affect the structure's natural period, this procedure was repeated until the natural period converged. The entire design process is briefly summarised in Figure 2. Tables 1 and 2 show the reinforcement adopted in both beams and columns. The clear cover adopted for both elements was 0.04 m. The reinforcement disposition was symmetric in order to take into account the reversal load situation due to seismic loads. The transversal reinforcement considered to calculate the effect of confinement on the section core was taken from the prescriptions in Eurocode 8 [24].

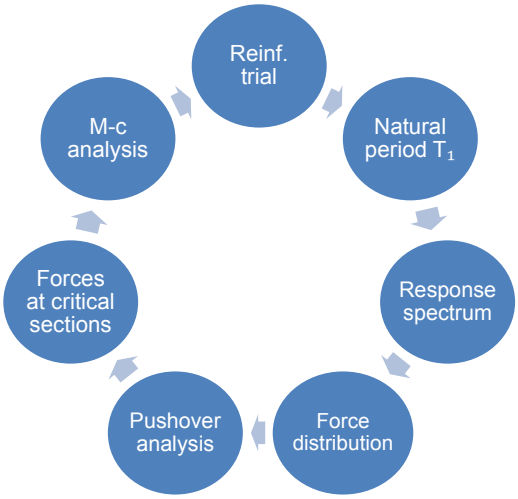

Figure 2. Reinforcement design procedure.

As seen in Tables 1 and 2, the design base shear V_{bd} reduced in the designs with SMA compared to their counterparts with steel. This was due to the natural period T_1 increment because of the SMA material's greater flexibility, which within that design spectrum range slowed down the design acceleration. Here we can also see that the improved concrete performance helped to cut the amount of the longitudinal reinforcement ratio ρ due to a reduction in the demand forces.

3. Finite element modelling.

3.1. Finite element model.

To carry out this study, the open access FEM software OpenSees [29] was used, which is particularly suitable for seismic analyses and to simulate earthquakes. To this end, the stress-strain models of the materials (concrete, steel and SMA-SE) proposed by other authors were implemented by the present authors into the Opensees material library. Thus the C++ language was utilised to write the code for the constitutive equations of the materials. The material parameters used in both the static pushover analysis and the dynamic analysis herein were calibrated by the authors with their own experimental data. The goodness of fit of the numerical models was verified using Opensees with the test results of the beam-column joints under cyclic loading tested by the research team (Pereiro et al. [2]). The stress-strain models of both concrete and steel were implemented by including both monotonic and cyclic behaviours. The behaviour of SMA was implemented according to the model of Lagoudas et al. [3], which takes into account the possible occurrence of residual deformations. In addition, the numerical model was validated with the other experimental results of structural elements by other authors (SMA RC bridge pier and SMA RC beams subjected to four-point bending tests).

Elements were modelled using the *displacement-based non-linear beam-column element*, which is included in the OpenSees element library. It is a 1D element of distributed plasticity based on the displacement formulation. The integration along the

element is based on the Gauss-Legendre quadrature rule [30]. In this study, seven integration points were used for both beams and columns. The behaviour at the section level at each integration point was studied by the fibre section approach, in which each section was discretised into fibres, to which the different constitutive behaviours were assigned. To represent the different behaviour of the confined core and concrete cover (with no confinement effect), two types of concrete materials were included in the concrete section. The area outside the stirrups was divided into four patches, and each was subdivided into 20 fibres on the sides, and into 30 fibres at the top and bottom of the section, to better capture the tension distribution on the compressed concrete top fibres and the concrete cracking on the tensile side. The core concrete was subdivided into 20x20 fibres. The discretisation choice was made iteratively so that reducing the number of fibres would not significantly affect the accuracy of the results while cutting the computing time. Rigid-links were introduced from the centreline to the face of the column to take into account the rigidity of joints.

In this work, the steel and SMA rebars were assumed to be connected using mechanical suitable couplers (Alam et al. [31], Haber et al. [32] and Nakashoji [33]). This study is preliminary research to explore the potential application of new materials (SMA and UHPC) in the design of MRF. For this reason, no special model was included to take into account the slippage of bars in mechanical couplers. Therefore in the model, no slippage occurred at the mechanical coupler and there was a perfect bond between all the reinforcement types and concrete materials. These hypotheses are a limitation for this work because, if the effect of slippage were significant, the results of this study could be modified. An improvement to the numerical model would include an equivalent zero-length moment rotational spring (Alam et al. [12], Billah and Alam [34] and Billah and Alam [26]) located at the end of the critical zones of either the beams or first floor supports (Figure 1). For this purpose, it is necessary to determine the slippage of the rebars inside the used coupler with a pullout test (Alam et al. [31]).

3.2. The material's constitutive equations.

Behaviour of SMA bars.

To define the behaviour of the SMA-SE bars in the numerical analysis, the experimental results of the tensile tests in the bars with diameters of 12 and 16 mm were used (Pereiro et al [2]). Tests were carried out at a room temperature (22°C). Since the temperature of the bar was expected to change during the loading process (self-heating during direct transformation, self-cooling during reverse transformation), a thermocouple was stuck to the bar face to control any temperature variations. The experimental results for a charge-discharge cycle of 3.5% deformation and a deformation rate of 1 mm/min can be found in Figure 3. In addition, a DSC test (Figure 4) was performed according to ASTM F2004-16 requirements to determine the four transformation temperatures, which were M_f = -49ºC, A_s =-21ºC, M_s = -31ºC, A_f = -8ºC. At a room temperature of 22ºC, the mechanical characteristics were σ^{Ms} = 389MPa, ε^{Ms} = 0.6% σ^{Mf} = 493MPa, ε^{Mf} = 5.1%, σ^{As} = 296MPa, ε^{As} = 4.7%, σ^{Af} = 187MPa, ε^{Af} = 0.3%.

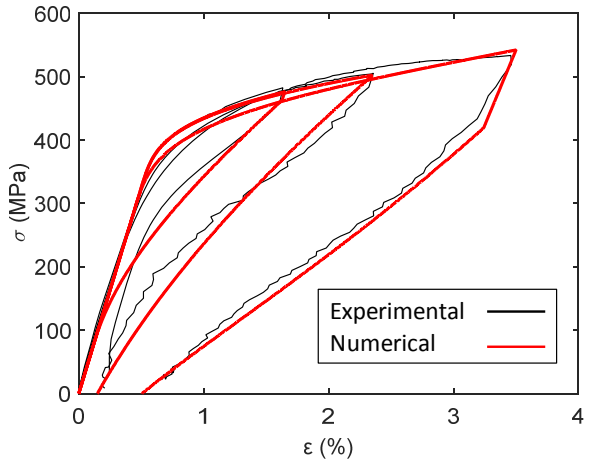

Figure 3. Loading-unloading cycle on a SMA-SE bar and the numerical model.

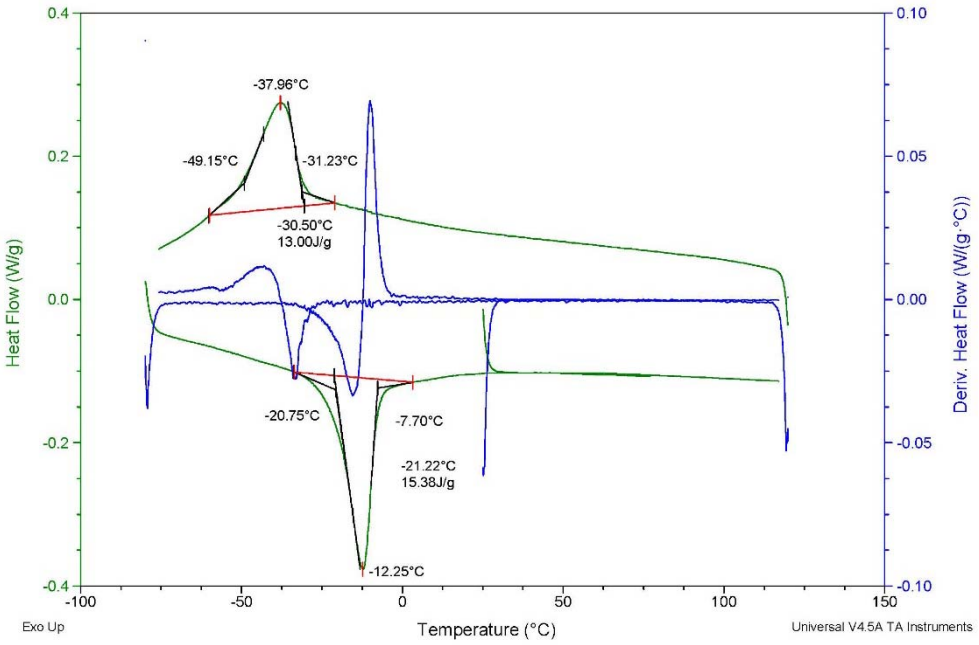

Figure 4. DSC experiment results (adapted from Pereiro et al [2]**)**.

The model developed by Lagoudas et al. [3] was implemented by the authors into the OpenSees material library as there was no default suitable material included in this software. This model takes into account the possible occurrence of residual deformations. The material's cyclic behaviour was also defined by including in the code the modifications for minor loops of Lagoudas and Bo [35]. This model was deduced from a theoretical thermodynamic framework. Given the thermomechanical coupling that characterises such materials, the main model parameters had to be obtained from both mechanical and thermal tests. Young's modulus in each phase and transformation strain H were obtained from a direct tension test, while the transformation temperatures, specific heat capacity of each phase and the specific entropy difference per unit volume $\rho\Delta s_0$ were deducted from a DSC test (Figure 4) [36]. The values obtained for the bars used in this research are shown in Table 3. The typical values of thermal expansion coefficients α_A and α_M found in the literature were used. In Figure 3, the model's goodness-of-fit is observed compared with the experimental results. A residual deformation of 0.5% was included in the model to adjust the experimental results.

Table 3. Values of the parameters used in the equation of Lagoudas et al [3] for NiTi bars SMA-SE.

α_A (K^{-1})	$11 \cdot 10^{-6}$
α_M (K^{-1})	$11 \cdot 10^{-6}$
E_A (MPa)	65000
E_M (MPa)	40000
H (%)	4
ρ (kg/m^3)	6500
c_A (J/m^3K)	600
c_M (J/m^3K)	600
M_f (ºC)	-49
A_s (ºC)	-21
M_s (ºC)	-31
A_f (ºC)	-8
$\rho\Delta s_0$ (MJ/m^3K)	-0.373

Behaviour of steel bars

To model the behaviour of the steel rebars, a new material was also implemented by the authors into the OpenSees material library, similarly to the Steel02 model included in OpenSees based on the Menegotto-Pinto model in cyclical behaviour terms, but with a plastic behaviour branch to better adjust the experimental results. The employed steel was commercial B500SD, which was tested in the laboratory with 540 MPa of actual yield strength, 650 MPa of ultimate strength and a Young's modulus of 200 GPa.

Concrete material modelling.

Three constitutive models were implemented by the authors into the OpenSees material library for the three concretes considered herein (NSC, HPC, UHPC), which were verified and calibrated with the experimental results, typical of compression tests done with cylindrical specimens.

For a conventional concrete with no embedded fibres and not confined, the model proposed by Model Code 2010 was used [37] up to a load drop of 5% (see Eq.(2)) was implemented by the authors into the OpenSees material library. The rest of the descending branch followed a linear branch until a residual tension of 5 MPa was reached.

$$\frac{\sigma}{f_{co}} = \frac{\beta\left(\varepsilon / \varepsilon_{co}\right)}{\beta - 1 + \left(\varepsilon / \varepsilon_{co}\right)} \tag{2}$$

where ε is strain, ε_{co} is the strain corresponding to compression strength f_{co}, σ is stress and β is a parameter that depends on the Young's modulus E_c and secant stiffness $(f_{co}/\varepsilon_{co})$:

$$\beta = \frac{E_c}{f_{co} / \varepsilon_{co}} \tag{3}$$

Figure 5.a shows the typical stress-strain relationship of a concrete specimen of normal strength, along with the fit obtained by the theoretical model. The behaviour of the confined concrete, for which no experimental results were available, was taken into account using the model proposed by Mander et al. [38] and implemented as such into OpenSees by the authors. The values of the parameters employed herein for confined and unconfined NSC are provided in Table 4, where f_t is tensile strength, f_{tr} is residual tensile strength and ε_{tr} is the corresponding tensile strain.

Table 4. Numerical values of the parameters for the constitutive models of the NSC material.

f_{co} (MPa)	ε_{co} (‰)	E_c (GPa)	f_t (MPa)	f_{tr} (MPa)	ε_{tr} (‰)	β
26.5	2.5	27.5	3.0	0.1	5	3.5

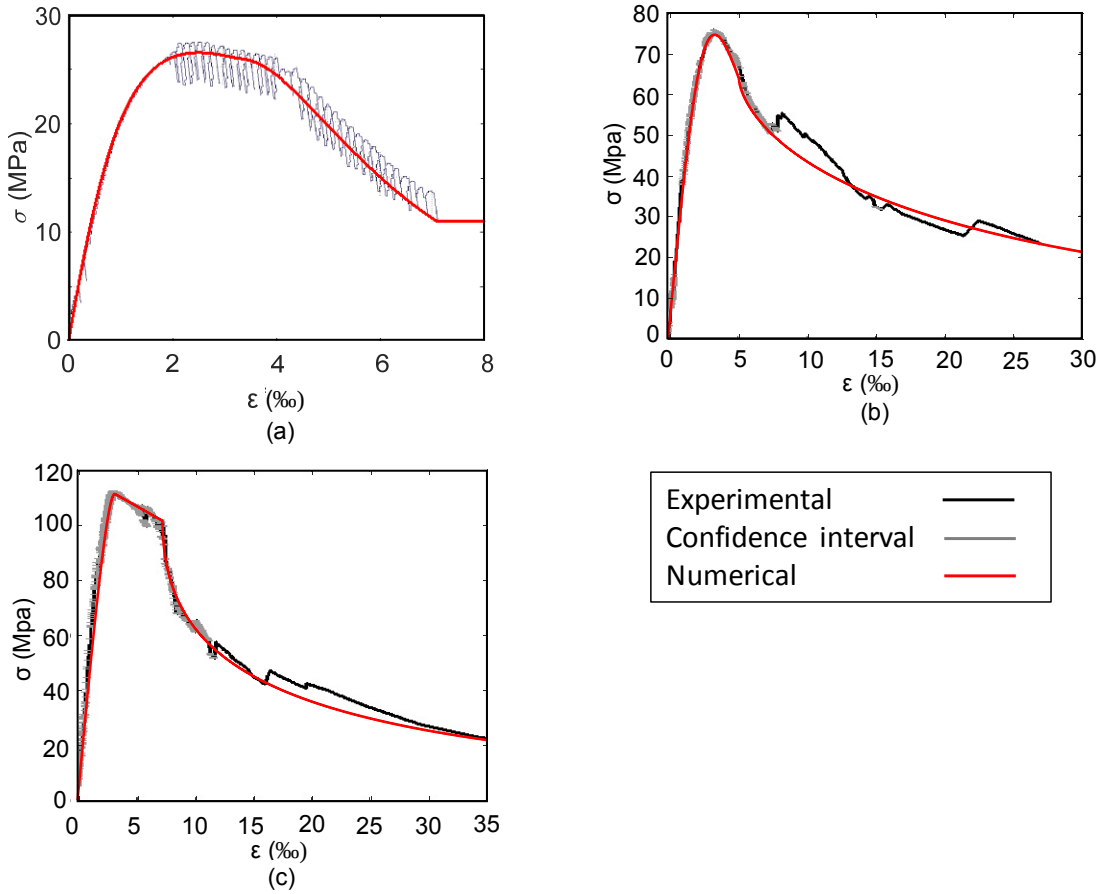

Figure 5. Experimental compressive stress-strain relationship tested and the implemented constitutive model by the authors for (a) NSC, (b) HPC and (c) UHPC with hybrid fibres.

The model implemented by the authors into OpenSees for HPC is based on the work of Campione [39], which considered the beneficial effect of steel fibres by reducing the actual distance between stirrups by a fictitious geometrical parameter that enhances the confinement effect. The ascending branch is based on the model proposed by Model Code 2010 [37], where β depends on fibre content:

$$\beta = A + B \cdot (RI)^C \tag{4}$$

where A,B and C are the fit parameters to the experimental results, and RI is the reinforcing index that depends on fibre content. For further references on the values of the fit parameters, see Campione [39]

The Model Code equation was used up to a certain normalised coordinate ($x_d = \varepsilon_d/\varepsilon_{co}, \eta_d = \sigma_d/f_{co}$), where the original envelope was replaced with an exponential curve:

$$\frac{\sigma}{f_c^{'}} = \eta_d \exp\left[-k_d\left(\frac{\varepsilon}{\varepsilon_0} - x_d\right)^{\gamma}\right] \quad (5)$$

where x_d, η_d, k_d depend on the steel fibre volume and the transverse reinforcement volumetric ratio. A value of 0.5 is recommended for γ, which controls curvature [39]. In Figure 5.b, the average stress-strain relationship of the seven HPC specimens and the fit using the model are shown. The effect of confinement was considered with the model proposed by Mander [38]. The values of the parameters used herein for the unconfined HPC are found in Table 5.

Table 5. Numerical values of the parameters for the constitutive models of the HPC material.

f_{co} (MPa)	ε_{co} (‰)	E_c (GPa)	x_d	k_d	γ	f_t (MPa)	f_{tr} (MPa)	ε_{tr} (‰)
74.8	3.4	35	1.52	0.3	0.65	5.0	0.2	5

Finally, the constitutive model implemented by the authors into OpenSees for UHPC was similar to that adopted for HPC, but an intermediate linear branch was added between peak resistance and the softening branch. For such a concrete type, the confinement effect that could arise from the stirrups was neglected. Figure 5.c shows the average stress-strain relationship for 14 specimens of the UHPC mixture reinforced with hybrid steel fibres and the adjustment by the theoretical model. It should be noted that both the ductility and strength for this mixture were superior. The values of the parameters used herein for UHPC are shown in Table 6, where f_t is tensile strength, f_{th} is the peak tensile strength at the end of strain hardening, ε_{th} is the corresponding strain and ε_{tu} is ultimate tensile strain.

Table 6. Numerical values of the parameters for the constitutive models of the UHPC material.

f_{co} (MPa)	ε_{co} (‰)	E_c (GPa)	f_{c1} (MPa)	ε_{c1} (‰)	k_d	γ	f_t (MPa)	f_{th} (MPa)	ε_{th} (‰)	ε_{tu} (‰)
116.5	3.2	46	75	7.5	0.75	0.5	10	12	8	55

Three-point flexural tests were carried out by Castro-Bugallo [16] and Pereiro et al [2] to determine the flexural behaviour of the analysed concrete mixtures. From these tests, and by means of a inverse analysis, the idealised behaviour in tension shown in

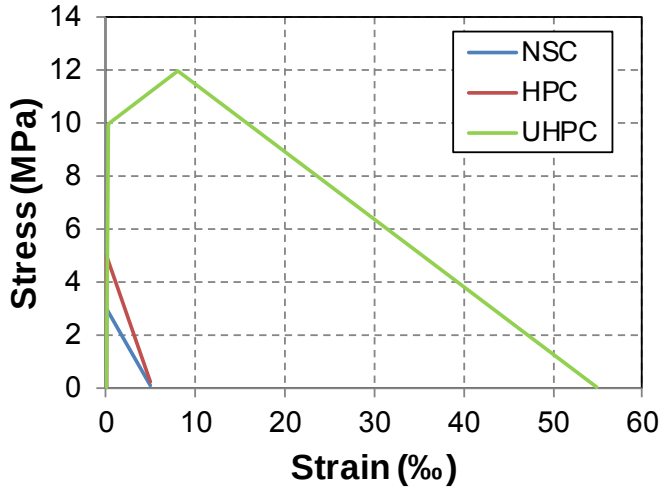

Figure **6** was obtained and later adopted for the models implemented by the authors into OpenSees. The values adopted for the tensile behaviour of the three concrete types (NSC, HPC and UHPC) can be found in Tables 4 to 6.

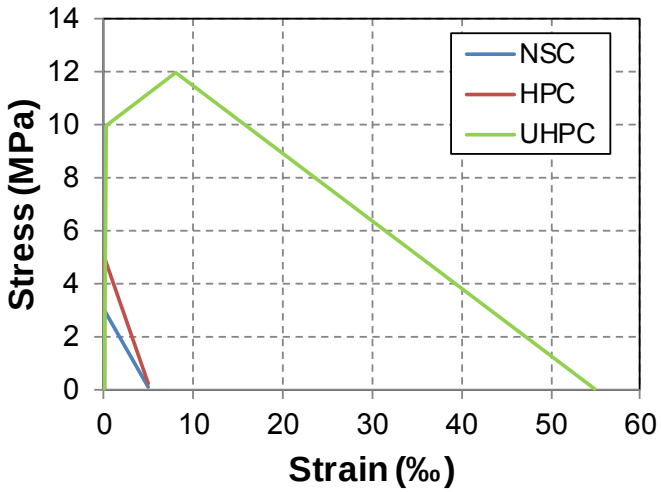

Figure 6. The tension stress-strain behaviour models for the three analysed concrete types.

Finally, in order to represent the cyclic behaviour of concrete, the approach by Mander et al. [38] was implemented by the authors into OpenSees for NSC. For HPC and UHPC, the loading and unloading branches proposed by Aslani et al [40,41] for high strength concrete were implemented by the authors into OpenSees.

Validation of the constitutive models.

To verify the suitability of the implemented constitutive models, the elements tested by Pereiro et al. [2] were simulated in OpenSees, which carried out cyclic tests of the beam-column joints manufactured with HPC and UHPC (Figure 7), and by replacing the conventional steel reinforcements with SMA in the plastic hinge area, whose estimated length was 600 mm from the face of the beam. The length of the tested elements was 3.3 m, which represents the distance between the points of zero bending moments of a building's inner column. The parameters analysed in this experimental programme were: concrete type (HPC or UHPC), relative normal force (ν) and transverse reinforcement spacing (s_t). Prior to the cyclic test, a relative normal force of 10-20% was applied depending one each case (see Table 7).

Table 7. Experimental programme by Pereiro et al. [2] carried out

Id	Specimen	Concrete type	Axial force (kN)	ν	s_t (mm)
C1	UHPC-V01S100	UHPC	497.68	0.10	100
C3	UHPC-V02S250	UHPC	940.17	0.20	250
C4	HPC-V01S100	HPC	302.08	0.10	100
C5	HPC-V02S100	HPC	644.76	0.20	100
C6	HPC-V02S250	HPC	655.84	0.20	250
C7	HPC-V03S100	HPC	937.32	0.30	100

Figure 7. Beam-column element tested in the laboratory (Pereiro et al. [2]).

Two types of concrete materials were used in this research. The first was a high-strength self-compacting concrete (HPC), whose average strength was 75 MPa, along with the addition of 80 kg/m^3 steel fibres. The second concrete mix was a ultra-high strength and self-compacting concrete reinforced with steel fibres (UHPC), with an average compression strength of 116 MPa. For both these two concrete types (HPC and UHPC), the experimental results from simple compression tests of cylindrical specimens were used to calibrate the numerical constitutive models implemented by the authors into OpenSees, whose summarised mechanical characteristics are provided in Table 8. The parameters of the constitutive model for SMA are those included in Table 3.

Table 8. Summary of the mechanical characteristics of the concrete used in [2].

	Specimen	f_{cm} (MPa)	E_c (MPa)	f_{LOP} (MPa	$f_{R,1}$ (MPa	$f_{R,2}$ (MPa)	$f_{R,3}$ (MPa)
C1	UHPC-V01S100	123.46	44415	11.30	19.06	17.54	12.85
C3	UHPC-V02S250	119.06	44366	10.04	17.51	16.70	13.85
C4	HPC-V01S100	75.03	35778	7.01	13.26	14.02	12.67
C5	HPC-V02S100	81.31	36234	7.82	15.17	16.27	14.21
C6	HPC-V02S200	84.00	36812	7.12	14.76	14.46	12.83
C7	HPC-V03S100	79.07	35629	6.18	11.67	12.65	11.02

Figure 8 provides the results of the numerical simulations of the real tested elements. In general, adjustment was quite accurate in terms of initial stiffness, monotonic envelopes and residual deformations for both elements constructed with UHPC (C1, C3) and HPC (C4 to C7). However, there were some limitations, such as the underestimated dissipated energy in element C1, the overevaluated dissipated energy in element C3 and the overestimated residual deformations in element C5.

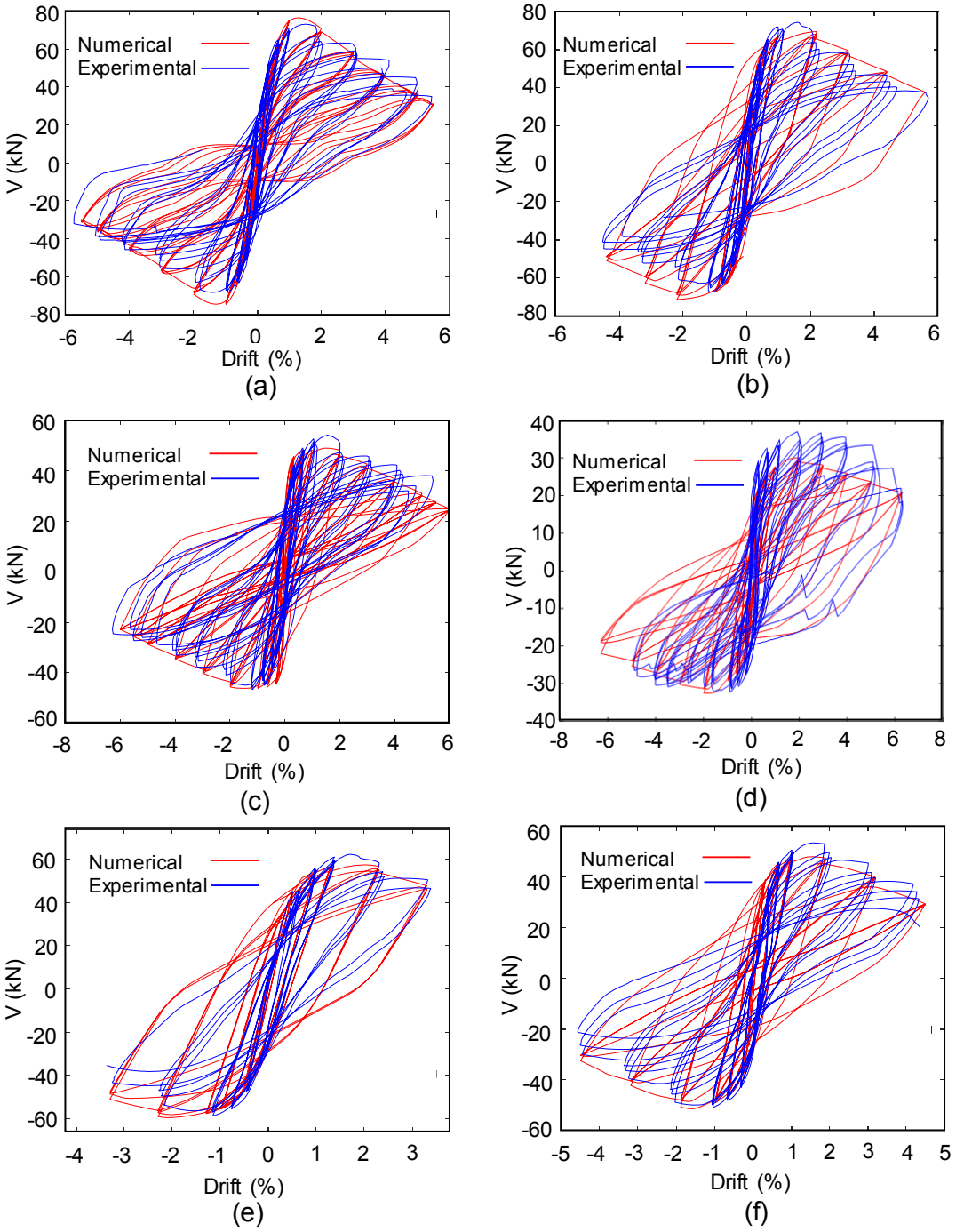

Figure 8. Results of the numerical simulations for the experimentally tested elements: (a) C1, (b) C3, (c) C4, (d) C5, (e) C6, (f) C7.

The authors also validated the implemented constitutive models by calibrating the experimental results obtained by other authors in different structural elements made of conventional concrete reinforced with superelastic SMA bars, and subjected to monotonic and cyclic loading. The experimental results obtained by Abdulridha et al. [8] on concrete beams reinforced with SMA and loaded at the midspan were adjusted

using the implemented models (Figure 9). Firstly, the SMA and concrete constitutive relationships were fitted to the quality control data provided by the authors (Figure 9.a). Secondly, the monotonic curve was adjusted with the finite element model (FEM) and on this basis of the cyclic curve (Figure 9.b-c). The numerical model allowed to properly simulate concrete cracking, residual deformations, ultimate load and unloading branches. Following the same process, similar performance was achieved in the experimental work by Saiidi et al. [42] for RC bridge piers reinforced with superelastic SMA bars and ECC in their critical zone (Figure 10). The control specimen, reinforced with conventional steel bars, was also adjusted as a reference.

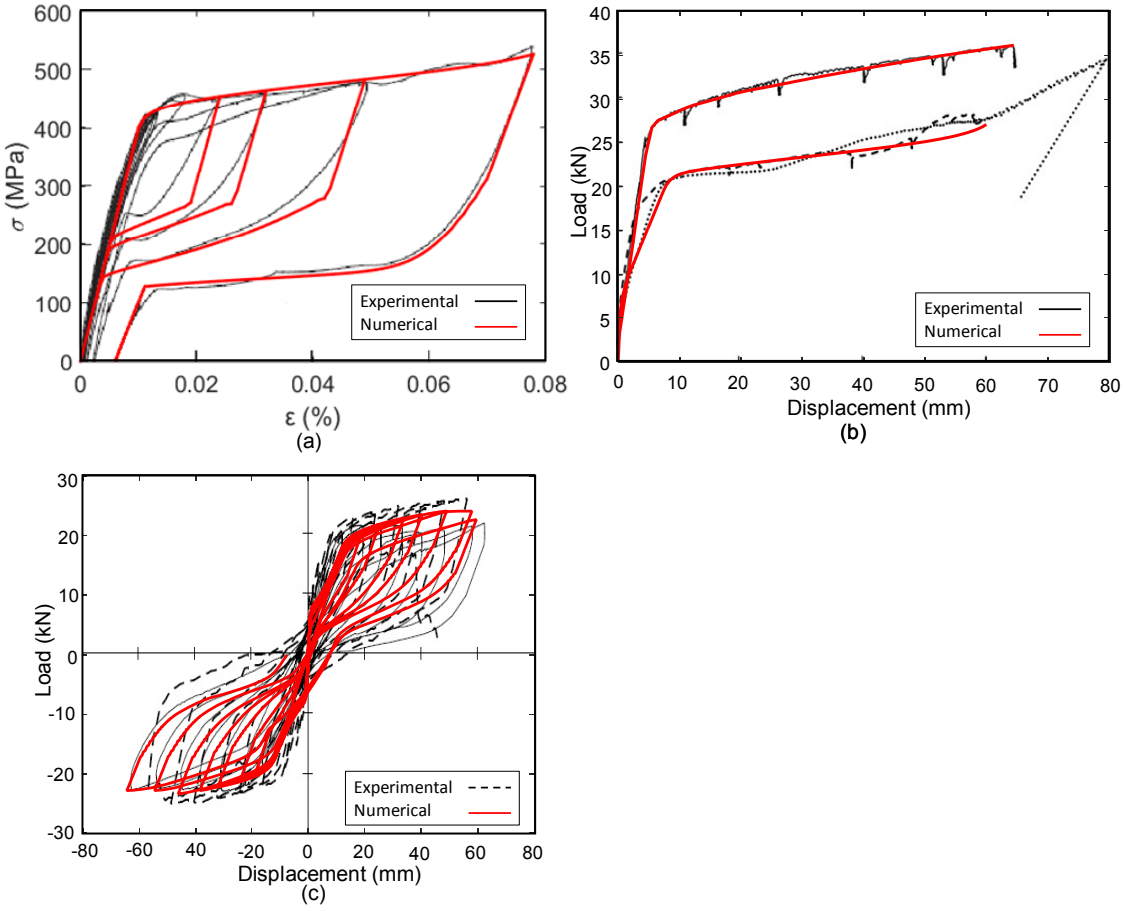

Figure 9. Comparison of the load-displacement relationship of the experimental (adapted from [8]) and predicted results in SMA RC beams: (a) The numerical SMA stress-strain relationship; (b) the monotonic load-displacement relationship: steel-reinforced beam (up), SMA-reinforced beam (bottom); (c) the cyclic load-displacement relationship.

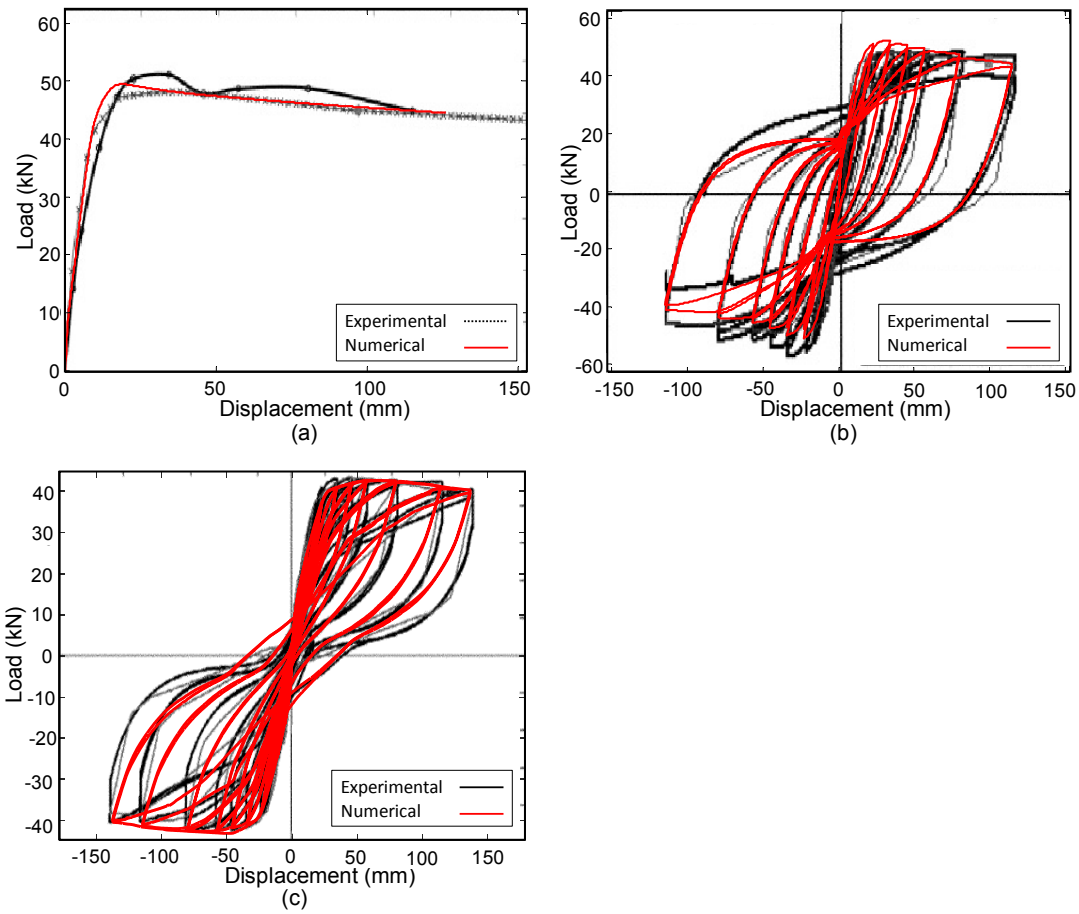

Figure 10. Comparison of the load-displacement relationship of the experimental (adapted from [42]*) and predicted results in SMA RC bridge piers: (a) the monotonic load-displacement relationship for the SMA RC specimen; (b) the cyclic load-displacement relationship for the steel RC specimen; (c) the cyclic load-displacement relationship for the SMA RC specimen.*

4. Static pushover analysis.

A non-linear static pushover analysis was carried out in OpenSees to analyse when the collapse mechanism occurred, and to derive the overresistance factors defined in the codes (Eurocode 8 [24], FEMA-695 [43]), such as the α_u/α_1 ratio between the multiplicative coefficients of the lateral loads that caused the formation of the first plastic hinge, V_{b1}, and for the building to become a global plastic mechanism, V_{bu} (see Figure 11):

$$\alpha_u / \alpha_1 = \frac{V_{bu}}{V_{b1}} = \frac{\alpha_u V_{bd}}{\alpha_1 V_{bd}} \quad (6)$$

the overstrength ratio Ω, which is the ratio between ultimate base shear V_{bu} and design base shear V_{bd}:

$$\Omega = \frac{V_{bu}}{V_{bd}} \tag{7}$$

and ductility, defined as the ratio between the drift corresponding to ultimate base shear Δ_u and the drift corresponding to first plastic hinge formation base shear Δ_1:

$$\mu = \frac{\Delta_u}{\Delta_1} \tag{8}$$

The pushover analysis was carried out on a static non-linear model that incorporated the non-linear constitutive behaviour of the materials and the distributed plasticity in elements. The properties of the materials were the same as those found in the previous section, except for the residual deformation of the constitutive curve for SMA, which was eliminated from the model for these numerical simulations as it was assumed that bars were fully trained before the construction and would not subsequently show any plastic deformation.

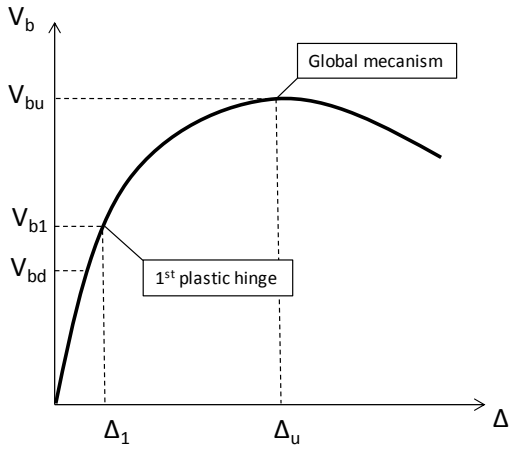

Figure 11. The typical base shear *vs.* the top drift pushover curve.

The formation of the first plastic hinge occurred on the beam end of the first floor for frame 3S1B, and on the beam end of the first or second floor depending on each case for frame 6S2B. The formation of the first plastic hinge was identified by the bending moment distributions along the elements at the time when the bending moment value was blocked, which indicated either the concrete's reinforcement yielding or its crushing. The maximum load $\alpha_u V_{bd}$ was reached at the moment in which enough plastic hinges were formed to convert the building into a global mechanism, which

occurred in all cases with the formation of a plastic hinge on the lower end of the first floor columns.

Figure 12 offers the results of this analysis, with the roof drift on the horizontal axis and the basal shear on the vertical axis, and the occurrence of the first plastic hinge and the global mechanism marked on the curves. Figure 10 illustrates how the initial rigidity increased with concrete strength and slightly reduced when SMA were used. In the three-storey building frames, the use of SMA delayed the formation of the first plastic hinge in drift terms for NSC (substantially) and for HPC, while for UHPC it accelerated the formation of the first plastic hinge. Regarding the global mechanism formation, HPC formation accelerated, while UHPC increased Δ_u.

In the six-storey building frames, increased concrete strength delayed the formation of the first plastic hinge. The effect on the global mechanism formation was the exact opposite to that mentioned above: improved concrete strength delayed this mechanism in the designs with steel, but advanced it in the designs with SMA.

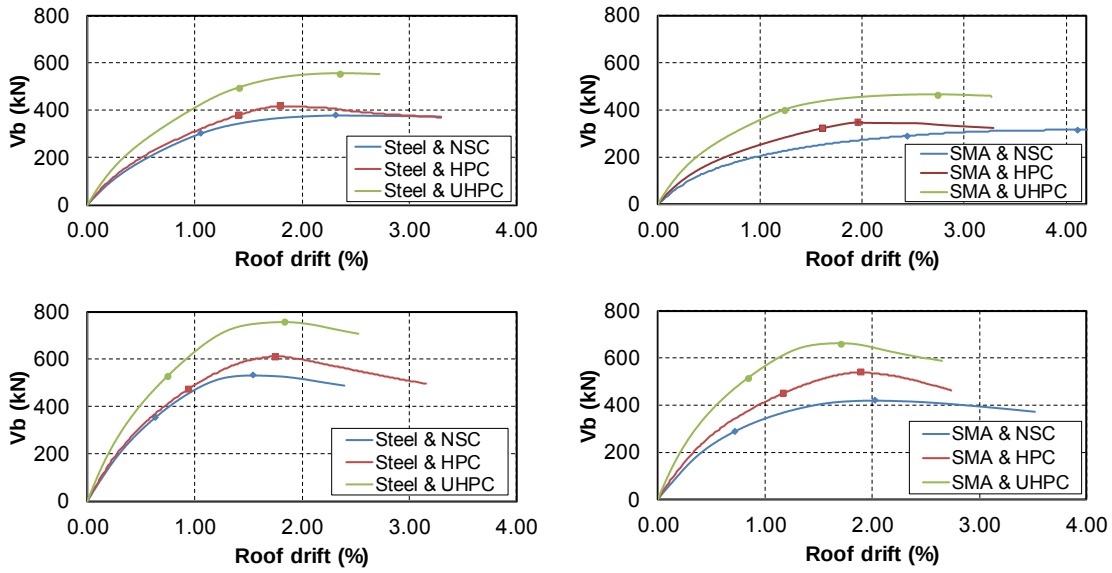

Figure 12. The static pushover analysis results: buildings 3S1B, steel design, (b) buildings 3S1B, SMA design, (c) buildings 6S2B, steel design, (d) buildings 6S2B, SMA design.

Table 9. The first plastic hinge and ultimate state base shear values and the overstrength factors for building 3S1B.

	Steel & NSC	SMA & NSC	Steel & HPC	SMA & HPC	Steel & UHPC	SMA & UHPC
$\boldsymbol{\alpha_u}V_{bd}$(kN)	378	315	418	347	556	465
$\boldsymbol{\alpha_1}V_{bd}$ kN)	300	289	379	327	492	400
V_{bd} (kN)	130	111	149	129	151	145
Ω	2.91	2.84	2.80	2.69	3.68	3.20
$\boldsymbol{\alpha_u/\alpha_1}$	1.26	1.09	1.10	1.06	1.13	1.16
$\boldsymbol{\Delta_1}$ (%)	1.04	2.43	1.41	1.65	1.39	1.24
$\boldsymbol{\Delta_u}$ (%)	2.30	4.11	1.80	1.96	2.37	2.74
μ	2.21	1.69	1.28	1.19	1.71	2.21

Table 10. The first plastic hinge and ultimate state base shear values and the overstrength factors for building 6S2B.

	Steel & NSC	SMA & NSC	Steel & HPC	SMA & HPC	Steel & UHPC	SMA & UHPC
$\boldsymbol{\alpha_u}V_{bd}$ (kN)	533	419	612	539	760	661
$\boldsymbol{\alpha_1}V_{bd}$ (kN)	351	289	475	453	520	514
V_{bd} (kN)	243	206	272	262	279	269
Ω	2.19	2.04	2.25	2.06	2.72	2.46
$\boldsymbol{\alpha_u/\alpha_1}$	1.52	1.45	1.29	1.19	1.46	1.29
$\boldsymbol{\Delta_1}$ (%)	0.63	0.71	0.94	1.18	0.73	0.84
$\boldsymbol{\Delta_u}$ (%)	1.54	2.01	1.77	1.90	1.83	1.69
μ	2.44	2.82	1.88	1.60	2.51	2.00

Overstrength coefficient Ω reaches higher values than 3 and was considerably higher in the three-storey building and the building modified with UHPC. This scenario was caused by the design requisite of a strong column weak beam, which considerably increased the capacity of columns in relation to that required by the design against gravitational loads, and delayed the formation of the global collapse mechanism, especially in lower buildings.

Regarding the α_u/α_1 ratio and as proposed by Eurocode 8 [24], the values obtained for the building with no design modifications (NSC, steel rebars) were consistent with this design code, which proposes values of 1.2 for one-bay and 1.3 for multi-bay buildings which, as seen, are conservative values, especially for 6S2B. However, the use of HPC significantly lowered the value of this coefficient given its lower ductility compared to

NSC. Using SMA also lowered the value of this coefficient in all but one case because it did not increase its tension as much as steel did after yielding. The use of UHPC brought about significant increases in the coefficient α_u/α_1 value, but did not reach the levels of the structures built with conventional concrete. As the value of this coefficient lowered, this meant that behaviour factor q was, in turn, lower. So for those forces whose corresponding linear-elastic system subject to these lateral loads would reduce less, it would be necessary to produce designs for higher equivalent lateral loads. However for the study period range, the increase in T_1 (see Tables 1 and 2) caused by lower SMA stiffness, V_{bd} also reduced and, hence, the use of SMA also had a beneficial effect.

Regarding ductility, the use of SMA in low-rise buildings reduced overall ductility because of its lower elastic modulus, which delayed the formation of the first plastic hinge. Ductility recovered in relation to the conventional design for the SMA and UHPC combination because the formation of the first plastic hinge accelerated by the early concrete failure instead of the yielding of SMA. Higher ductility values were obtained for building 6S2B due to its greater redundancy. Except for NSC, in which the use of SMA was advantageous given the delay in collapse mechanism formation, in the other cases SMA delayed the formation of the first plastic hinge by reducing ductility altogether. For both 31SB and 62SB, the use of HPC was detrimental for overall ductility, and the use of UHPC enhanced its value.

5. Dynamic analysis.

A dynamic analysis was carried out in a time domain to analyse and compare the seismic behaviour of the prototypes modified with different materials. The incremental dynamic analysis (IDA) procedure was followed, in which the accelerogram was increasingly scaled similarly to that done with the lateral load in a static non-linear pushover analysis, with similar results in both analyses. To run the analyses, the Rayleigh method was used by considering 5% critical damping, which was proportional

to both the mass matrix and the rigidity matrix updated at each instant. At the end of the analysis, prototypes were left for 10 s in a free vibration situation, as indicated by Eurocode 8 [1].

5.1. Properties of the analysis ground motions.

For this study, a set of six real accelerograms was taken. Although Eurocode 8 establishes the use of a minimum of three ground motions, three more were taken into account to obtain a certain degree of heterogeneity in order to evaluate the validity of the designs for a wider set of earthquakes, instead of using only ground motions that are representative of the site. For this purpose, two accelerograms were chosen with low (<0.8) PGA/PGV ratio values, where PGA is Peak Ground Acceleration and PGV is Peak Ground Velocity. Two took medium PGA/PGV ratio values (0.8-1.2) and two had high PGA/PGV values (> 1.2), as recommended by Alam et al. [12], whose detailed parameters are shown in Table 9, where T_{eq} is the predominant period of the response spectrum for 5% damping, whose representation appears in Figure 13.

Table 11. Characteristics of the selected ground motions.

Ground motion	Date	Station	Magnitude	PGA (g)	PGV (m/s)	PGA/PGV	T_{eq} (s)
Chi-chi (Taiwan)	2008	CHY 006	7.62	0.358	0.56	0.64	0.46
Tabas (Iran)	1978	Tabas	7.35	0.812	1.14	0.72	0.24
Kocaeli (Turkey)	1999	Fatih	7.51	0.175	0.18	0.96	0.54
Loma Prieta (USA)	1989	Coyote Lake Dam - Southwest Abutment	6.93	0.343	0.31	1.11	0.64
L'Aquila (Italy)	2009	L'Aquila - V. Aterno - Centro Valle	6.3	0.558	0.41	1.37	0.2
Kozani (Greece)	1995	Kozani	6.4	0.16	0.08	2.07	0.2

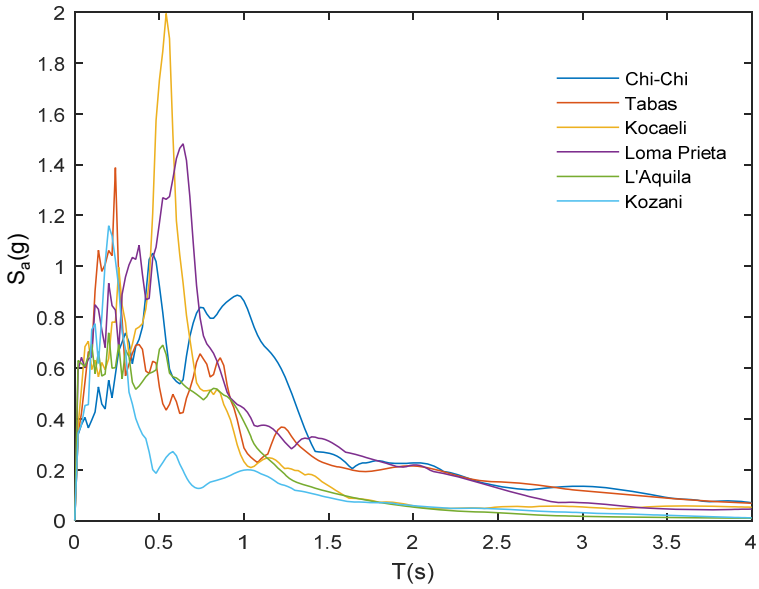

Figure 13. Response spectra (5% critical damping) for the ground motions selected for the study.

5.2. Incremental Dynamic Analysis (IDA) curves.

In Figures 12 and 13, the IDA curves are respectively shown for buildings 31SB and 6S2B. These curves were obtained by submitting all 12 prototypes (Tables 1 and 2), subjected to the six selected ground motions (Table 11), and scaled to the PGA shown in the ordinates. On the abscissa, the maximum occurred interstorey drift (IS drift) is represented. Earthquakes were scaled up to 2.5 g, shown in the graphs for each design until the maximum acceleration prior to collapse. It should be noted that no building collapsed by design acceleration.

For the low-rise building frames, the interstorey drift did not seem to present any clear pattern because the structure's natural period, of around 0.55 s, came very close to the predominant period of some earthquakes, which amplified the response for those designs that modified the structure's period to move towards the value of the predominant period of the response spectrum. In Figure 12, two cases of collapse (Chi-Chi, Lomaprieta) are observed for the standard building (steel and NSC), possibly due to the proximity of their natural frequencies to the frequency content of the response spectrum. For the building reinforced with SMA and NSC, two ground motions are

observed (Chi-Chi and Tabas), which SMA reached in the martensitic state, in which stiffness once again rapidly increased (see Figure 6) and helped control interstorey drifts. The same can be stated for the SMA and HPC combination for both Tabas and L'Aquila. Similar phenomena wer found for building 6S2B, as seen in Figure 13 for the NSC and SMA combination (Tabas, Lomaprieta) and for the UHPC and SMA combination (Chi-Chi, Tabas) which, in this case, was because the failure section moved outside the critical zone and the NSC section capacity was exceeded.

With building 6S2B, whose natural period was roughly 1.1 s, we can see that interstorey drift reduced if HPC or UHPC was used, but increases when steel bars were replaced with SMA bars in the structure's critical zones as both changes modified the structure's rigidity in one direction or another.

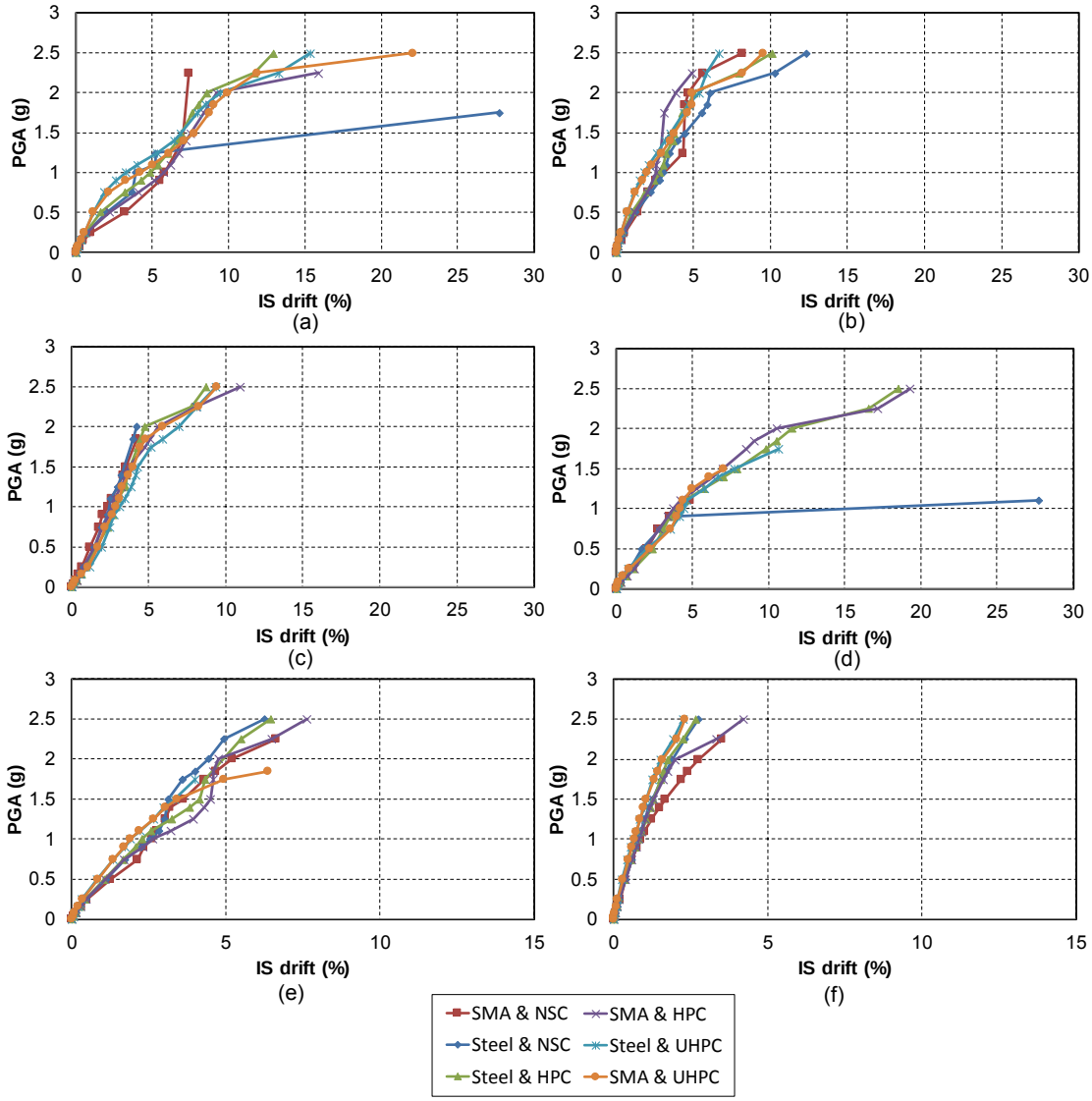

Figure 14. IDA curves for building 3S1B: (a) Chi-Chi; (b) Tabas; (c) Kocaeli; (d) Lomaprieta; (e) L'Aquila; (f) Kozani.

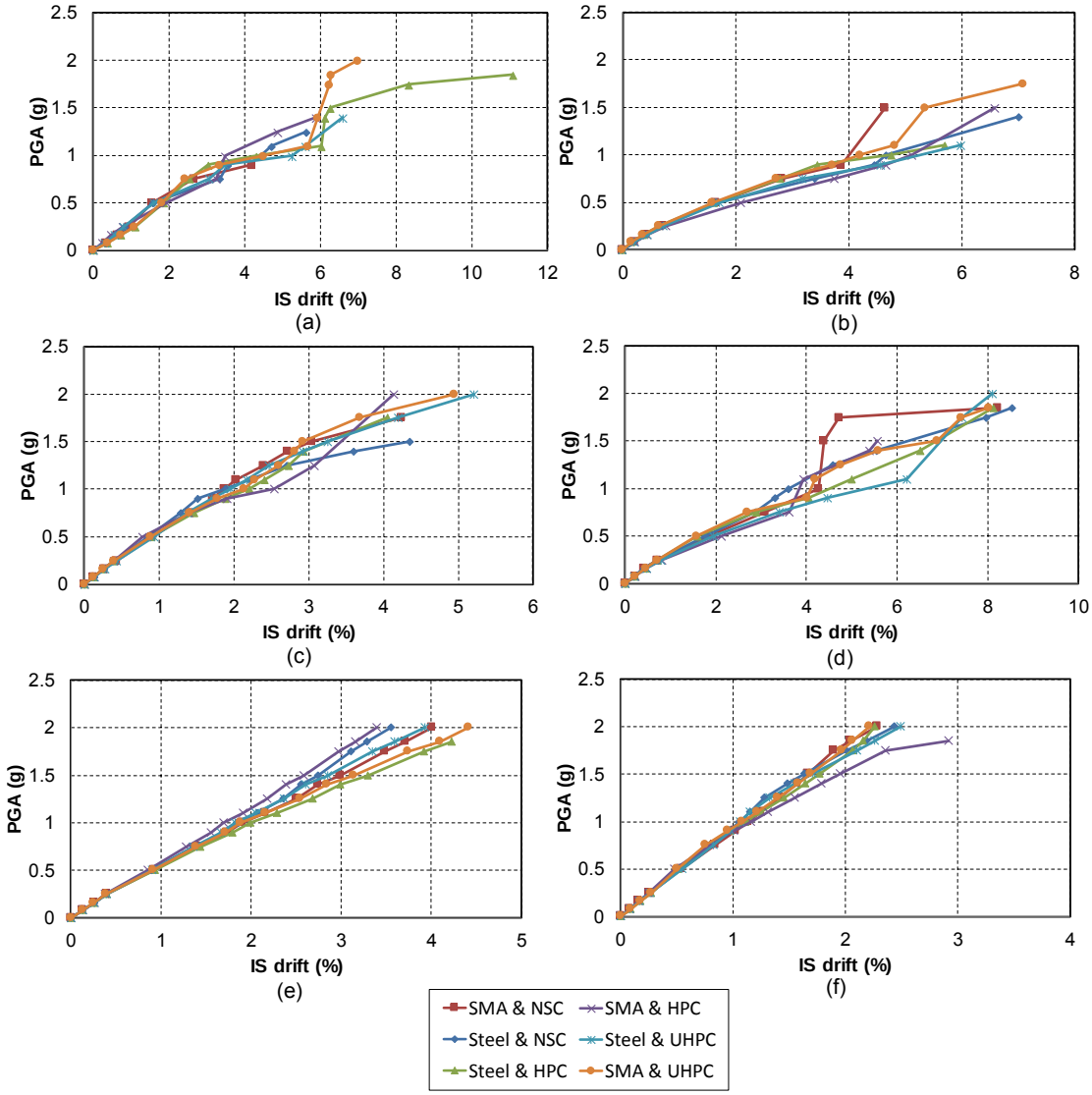

Figure 15. IDA curves for building 6S2B: (a) Chi-Chi, (b) Tabas; (c) Kocaeli; (d) Lomaprieta; (e) L'Aquila; (f) Kozani.

Finally, it is worth mentioning that the maximum drift between storeys normally occurred at the first or second floor in all the buildings, which led to a great demand in drift terms, especially in the buildings reinforced with SMA in critical zones. Figure 14 depicts building 3S1B constructed with NSC, reinforced with steel (a) and with SMA-SE in critical areas (b) for comparison purpose, showing that SMA significantly increases the drift demand of at the first and second floors.

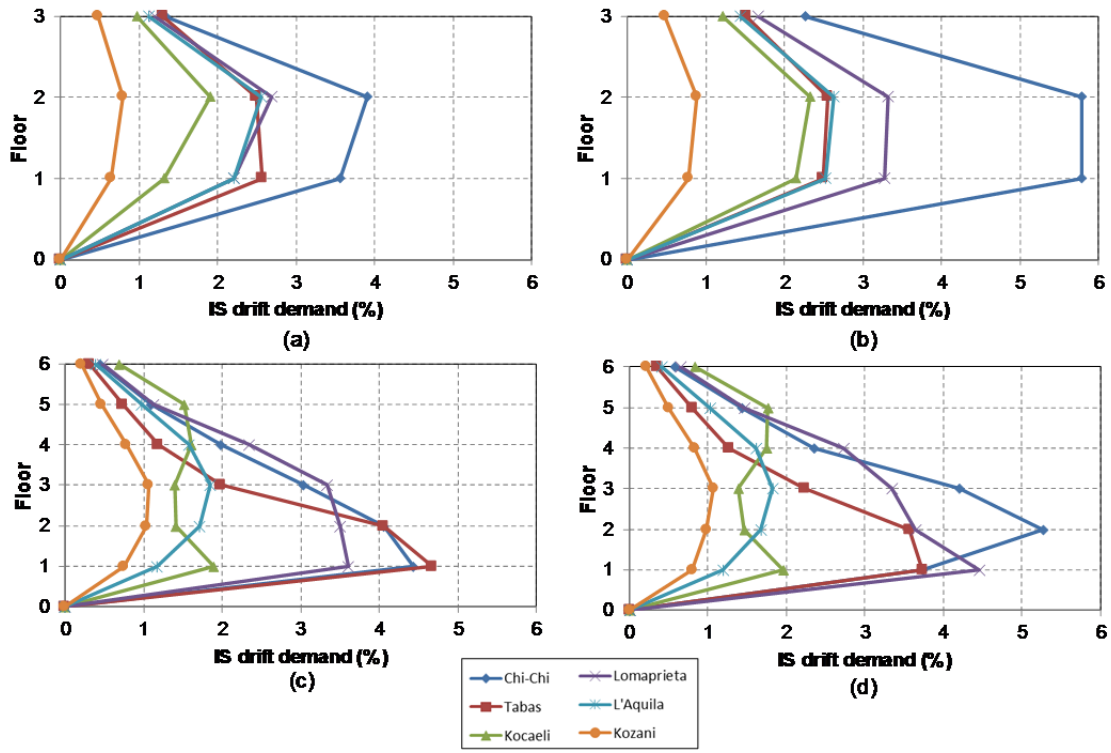

Figure 16. IS drift demand for building 3S1B NSC: (a) reinforced with steel, (b) reinforced with SMA-SE in critical zones; and for building 362B NSC: (c) reinforced with steel, (d) reinforced with SMA-SE in critical zones.

5.3. Base shear *vs.* maximum roof drift pushover curves.

In this section the dynamic pushover curves were built, in which the maximum basal shear *vs.* the maximum roof drift are represented for each MRF design (Tables 1 and 2), subjected to the set of earthquakes indicated in Table 11. Each pushover curve point corresponding to an MRF and ground motion scaled to increasing PGAs represents the maximum response in basal shear-drift terms for a given PGA.

The dynamic pushover curves represent the maximum roof drift against the corresponding basal shear, similarly to the representation of a static pushover analysis. However, the result is different because in the building's dynamic response, both the frequency content of the ground motion and the building's dynamic characteristics (mass distribution, rigidity, etc.) influence the response. That is why the building's dynamic capacity is not unique, but depends on the applied ground motion, in the same way as the backbone of a pushover analysis depends on the distribution of lateral

loads. The intention of using several different ground motions is to determine the structure's capacity against a wider variety of earthquakes. Figure 15 and Figure 18 respectively show the results of the dynamic simulation for the designs made for buildings 3S1B and 6S2B. Substantial variations in the response are observed, especially for the cases of Kocaeli, whose natural period comes close to that of the 3S1B structure, and L'Aquila, whose duration is longer. The variation in the response is narrower for building 6S2B due to the higher degree of the structure's redundancy, also to and a long natural period, far from the predominant period of the analysed ground motions. The Kozani earthquake barely excited building 3S1B or building 6S2B because its frequency content was distributed far from the building's natural frequency.

In general, and as expected, the buildings modified with UHPC have a greater capacity and initial rigidity, unlike the buildings reinforced with SMA, with much less initial stiffness and capacity. This is more noticeable in the buildings reinforced with NSC because concrete is unable to cope with SMA deformations, the concrete compression block fails and cover spalling occurs, as deduced from the results of the numerical simulation at the sectional level. In some cases for SMA with HPC, such as Lomaprieta for 6S2B, L'Aquila for 3S1B, or for SMA with UHPC, such as Kocaeli for 3S1B and Kozani for 3S1B, SMA enter the martensitic strain range and are able to once again increase their resistant capacity. Although this constitutes an emergency resistance reserve for the most intense earthquakes, it is not desirable in general as non-recoverable plastic deformations can be induced in SMA by the martensitic phase yielding, and using SMA bars intends to avoid this. In building 6S2B, for the majority of the analysed ground motions, the UHPC with SMA combination presented greater capacity than that with steel thanks to it better accommodating the movements imposed by the earthquake and cuasing less damage in critical zones.

In general terms, both buildings 3S1B and 6S2B develop a greater resistance capacity for earthquakes with a low PGA/PGV ratio. The buildings designed with SMA and NSC

presented the least capacity and equivalent rigidity, while the buildings designed with UHPC offered the best rigidity and capacities. With building frames 3S1B, UHPC with steel presented greater capacity, as in the static analysis, while buildings 6S2B displayed greater capacity for designs with SMA and UHPC, unlike the static analysis.

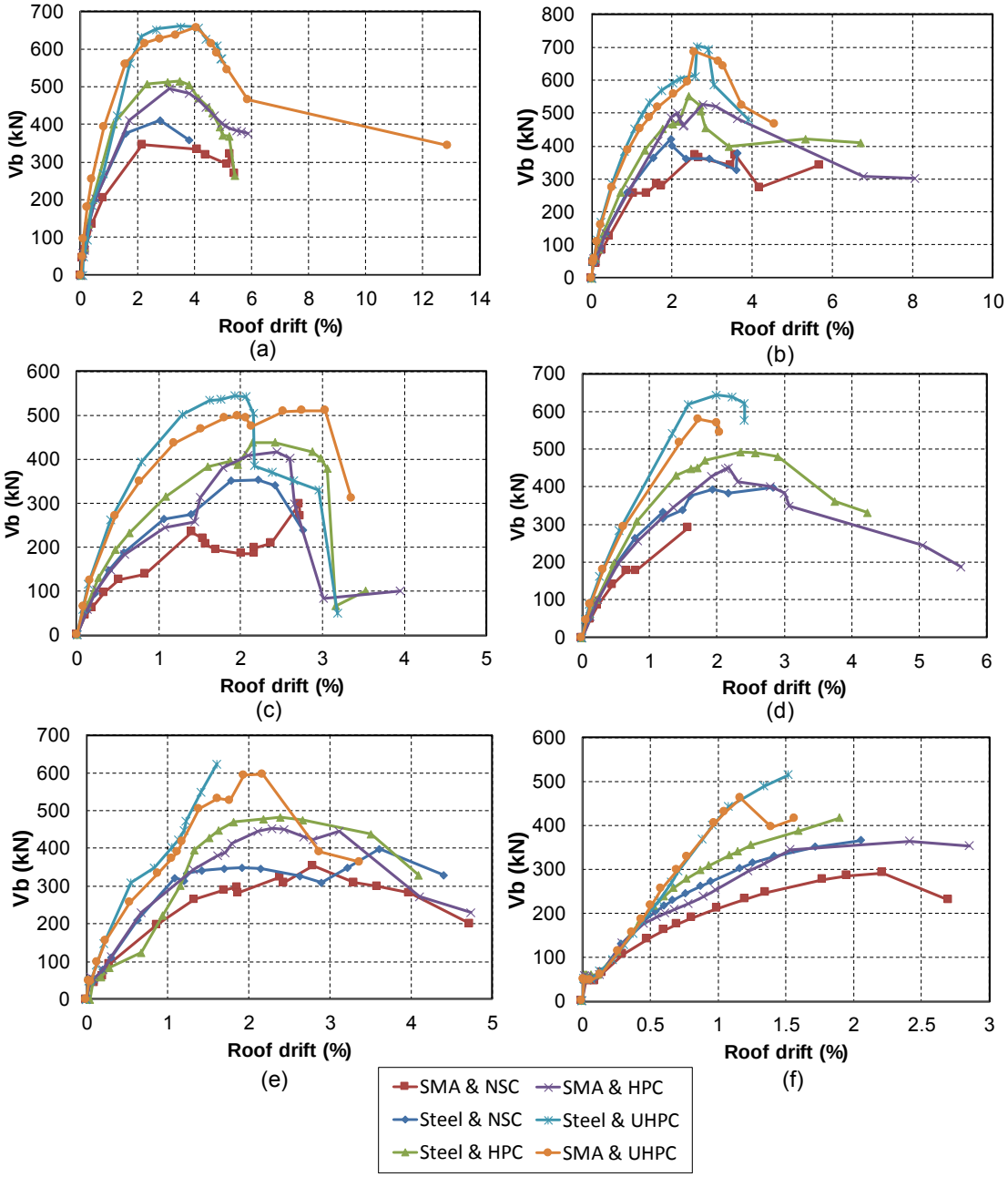

Figure 17. IDA pushover curves for the different building 3S1B designs: (a) Chi-Chi; (b) Tabas; (c) Kocaeli; (d) Lomaprieta; (e) L'Aquila; (f) Kozani.

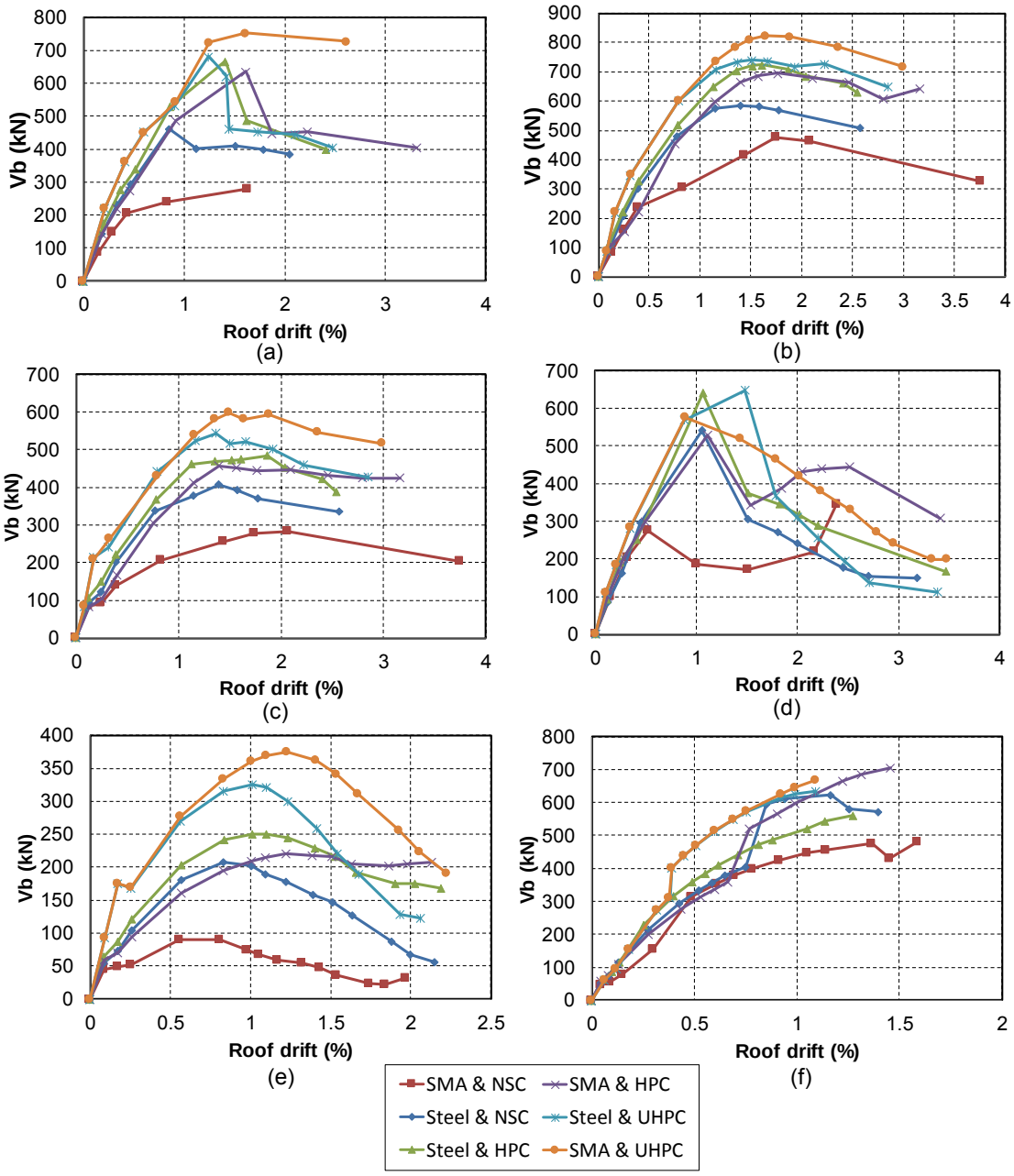

Figure 18. IDA pushover curves for the different building 6S2B designs: (a) Chi-Chi; (b) Tabas; (c) Kocaeli; (d) Lomaprieta; (e) L'Aquila; (f) Kozani.

5.4. Residual drifts.

Figure 19 and Figure 20 illustrate the maximum residual interstorey drifts that resulted from applying the accelerogram to each PGA level. Drifts were calculated by considering the maximum residual drift of all the storeys for the ground motions that finished without collapsing and, for the cases in which collapse occurred, as the maximum drift in the last step with a null base shear value.

In general, standard buildings 3S1B have higher residual drifts than 6S2B ones. Replacing conventional steel reinforcements in critical areas with SMA reduces deformations by an average of 66%. We can see that for the SMA combination with HPC and UHPC, average reductions of 90% in the residual drift were obtained with a conventional design using NSC and steel, and the best performance was that which corresponded to UHPC with SMA in most cases due to the recentering capacity of SMA. It should be noted that the buildings reinforced with SMA had higher drifts during ground motions than those buildings reinforced with steel. For the majority of 6S2B buildings, the generation of plastic deformations started at around 0.75-1g, while wider variability was achieved for 3S1B buildings, depending on the earthquake and the design type.

In some cases, the SMA RC frames show larger residual interstorey drifts for a certain PGA range than their reinforcing steel counterparts. The rationale for this lies in the fact that the length for provided the critical zone is insufficient for thrse material-ground motion combinations. This results in failure at the joint section due to lack of resistant capacity, and also in the subsequent accumulation of residual deformations. To avoid this behaviour, the critical length should be adjusted for these combinations. In further research works, an optimal critical length for a set of different ground motions will be taken into account.

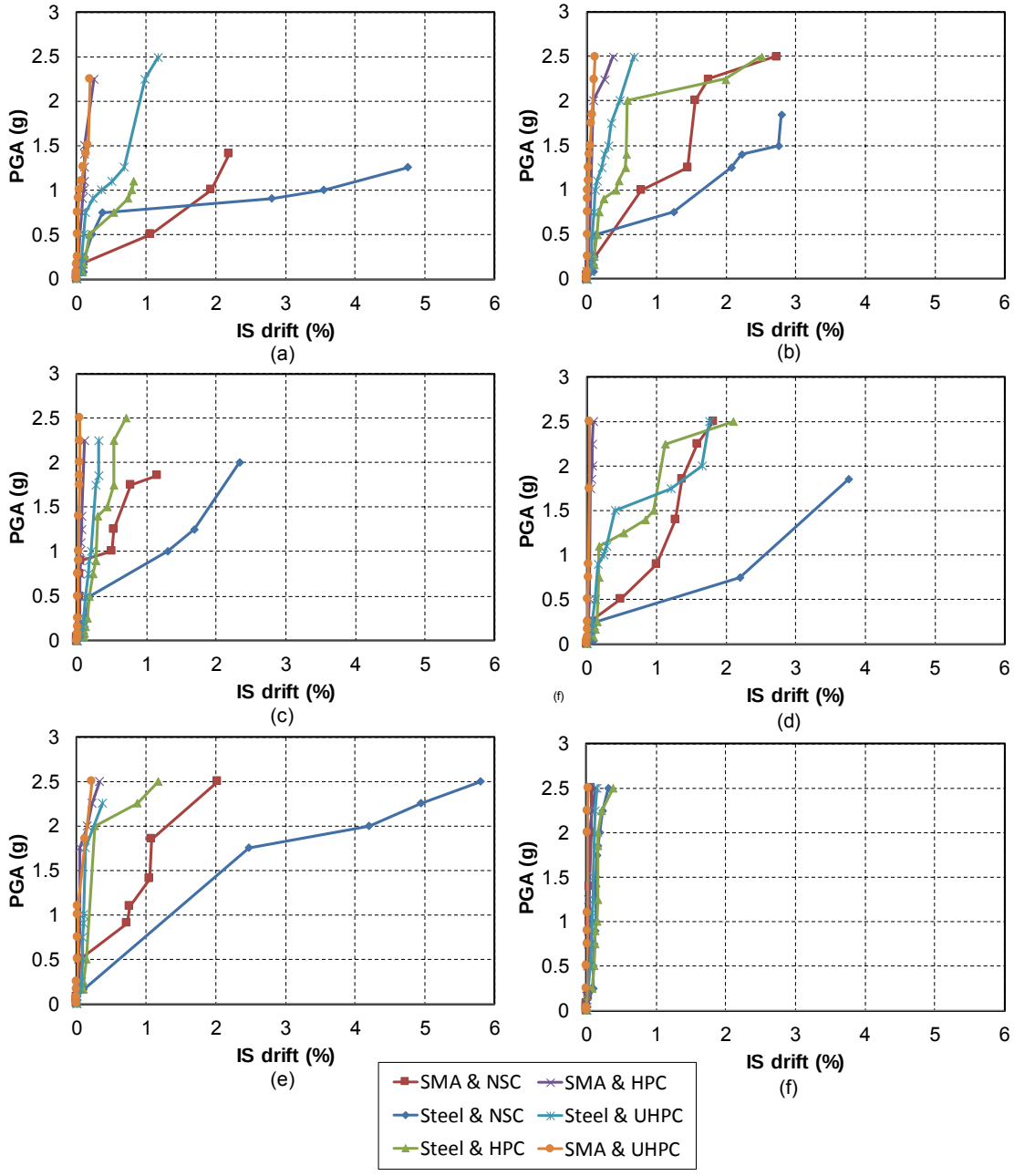

Figure 19. Residual interstorey drifts for building 3S1B: (a) Chi-Chi; (b) Tabas; (c) Kocaeli; (d) Lomaprieta; (e) L'Aquila; (f) Kozani.

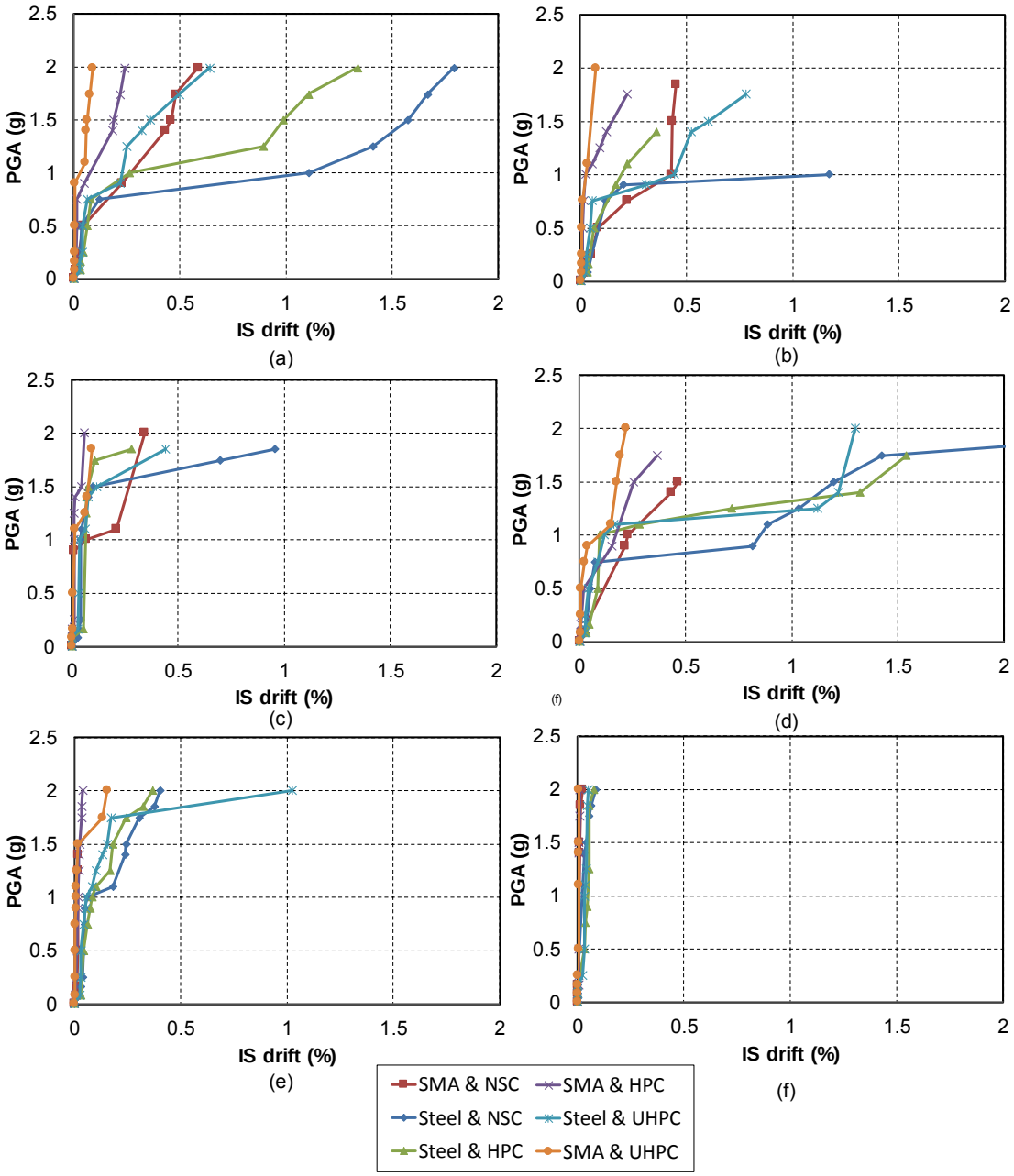

Figure 20. Residual interstorey drifts for building 6S2B: (a) Chi-Chi; (b) Tabas; (c) Kocaeli; (d) Lomaprieta; (e) L'Aquila; (f) Kozani.

6. Response modification factors.

This section analysed the seismic response factors for the studied buildings. It started with the generic definition of these parameters by American design codes (UBC [44], ASCE/SEI 7-05 [45]), whose values were compared to those established by Eurocode 8 [24]. See Figure 21 for a graphical understanding of the meaning of several factors.

CVodes introduce the behaviour factor by which the stresses that could result from an elastic calculation can reduce through reduction factor R:

$$R = \frac{V_E}{V_{bd}} \tag{9}$$

where V_E is the base shear demand of the equivalent linear-elastic building model.

That is, it allows the base shear to lower, which would be necessary for the structure to remain within the elastic range during an earthquake. This reduction factor can be decomposed into the overstrength factor (calculated before), which accounts for the code requisites that increase real capacity in relation to the actual demand (load safety factor, material safety factor, real disposed reinforcement, other global and local requisites, etc.), and ductility reduction factor R_μ.

$$R_\mu = \frac{V_E}{V_u} \tag{10}$$

This factor R_μ relates the elastic force demand of an elastic response spectrum with the building's actual capacity. This factor is discussed in this section.

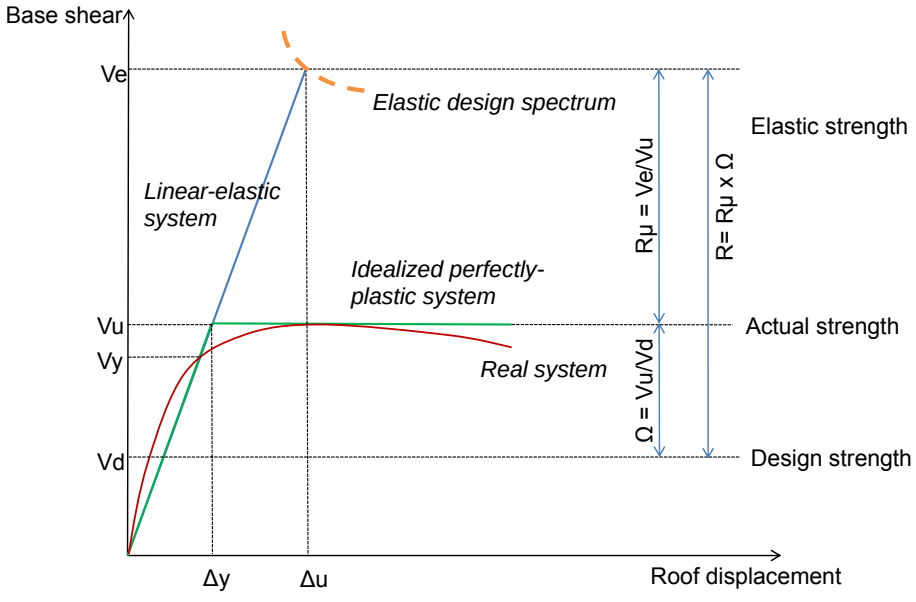

Figure 21. Graphical definition of the seismic performance factors.

Reduction factor R_μ was calculated by following a purely dynamic approach that is consistent with the normal definitions of the reduction factor for 1dof systems (see

Chopra [46] for further details) by an analogy to mdof systems, and following a similar methodology to that os Gerami et al. [47]. For this purpose, the structure's real capacity was taken from the IDA curve results from the previous section and not from a conventional static pushover curve. The corresponding elastic force was taken following the same IDA process in a perfect elastic-linear system modeled in OpenSees by the Elastic Beam-Column element with the homogenised area and inertia, and the same mass distribution. Previous earthquakes were applied to this system and were scaled with increasing PGAs, analogously to the previous section. The obtained results are shown in Table 12 for building 3S1B and in Table 13 for building 6S2B. The Kozani ground motion was removed from the analysis as it failed to completely excite the building.

Table 12. R_μ factors for building 3S1B.

	Steel & NSC		SMA & NSC		Steel & HPC		SMA & HPC		Steel & UHPC		SMA & UHPC	
	V_E (kN)	R_μ	V_E (kN)	R_μ	V_E (kN)	R_μ	V_E (kN)	R_μ	V_E (kN)	R_μ	V_E (kN)	R_μ
Chi-chi	928	2.26	592	1.72	1210	2.35	931	1.88	1171	1.77	1433	2.17
Tabas	764	1.81	862	2.32	982	1.78	1312	2.49	1516	2.15	1213	1.77
Kocaeli	937	2.66	1361	5.82	986	2.25	2046	4.91	1166	2.14	2334	4.57
Lomaprieta	1069	2.69	1550	5.33	1020	2.07	1595	3.54	844	1.31	666	1.15
L'Aquila	822	2.35	1056	2.99	943	1.95	874	1.93	876	1.40	1083	1.81
$\bar{R}_\mu$		2.35		3.63		2.08		2.95		1.76		2.29
C.V. (%)		15.2		50.5		11.0		43.5		22.6		57.7

Table 13. R_μ factors for building 6S2B.

	Steel & NSC		SMA & NSC		Steel & HPC		SMA & HPC		Steel & UHPC		SMA & UHPC	
	V_E (kN)	R_μ	V_E (kN)	R_μ	V_E (kN)	R_μ	V_E (kN)	R_μ	V_E (kN)	R_μ	V_E (kN)	R_μ
Chi-chi	1676	3.64	914	3.26	2608	3.90	2406	3.78	2810	4.13	3203	4.26
Tabas	1028	1.76	1417	2.97	1316	1.81	1182	1.70	1411	1.91	1435	1.74
Kocaeli	1045	2.54	1021	3.55	1225	2.52	1310	2.82	1465	2.67	1410	2.31
Lomaprieta	734	1.35	1330	3.86	801	1.25	679	1.28	1414	2.19	894	1.55
L'Aquila	931	4.48	819	9.00	1278	5.11	1333	6.03	1352	4.15	1560	4.17
$\bar{R}_\mu$		2.75		4.53		2.92		3.12		3.01		2.81
C.V. (%)		47.2		55.7		54.0		60.8		35.4		46.9

As factor R_μ was related intrinsically to the structure's ductility, the combinations with SMA presented higher R_μ coefficient values in most cases than the corresponding ones reinforced with steel. It was observed that the SMA and NSC combination proved to be

the most efficient in producing the weak first floor mechanism. Hence in some cases it entailes a significant reduction in the acting forces on the structure, and reached values of 9. With UHPC with SMA, it did not seem to work optimally as the damaged zone was outside the plastic hinge area by transferring the failure mechanism to the area with the worse concrete. Consequently, a longer critical length or better concrete was necessary in the continuation of the critical zone. More attention should be paid to this aspect in future applications. In general, the R_μ coefficient values were around 20% higher for the higher-rise building with more bays.

Using overresistance factors Ω as defined above, we obtained the global reduction factor R, analogously to behaviour factor q of Eurocode 8. The obtained values are found in Table 14. If an R value of UBC-97 was considered valid, with one of 5.5 for "Concrete intermediate moment-resisting frames", the design achieved through Eurocode 8 for building 6S2B would be non-conservative. However, q values of 3.6 and 3.9 were taken for the buildings without and with bay redundancy, which are very conservative values in view of the results for both buildings made with steel and NSC. The R value is significantly affected by height, and was higher for the lower buildings without redundancy, which is the opposite to EC-8. In addition, the optimal combination to reduce efforts was not the same according to building type, where the best was SMA with HPC for low-rise buildings and SMA with UHPC for mid-rise buildings.

In conventional RC buildings, it can be generally stated thay the stiffer the frame, the higher the R factor value [48]. According to the present results, this rule is still fulfilled for changes in geometry or concrete resistance. However, the introduction of SMA into the design also increases the R factor (39% for 3S1B, 8% for 6S2B) via two mechanisms: the martensite resistant reserve and the intrinsic ductility of SMA. UHPC also has a positive effect on the R factor value compared to the designs with NSC, and this effect being especially notable on 6S2B frames (27% on average).

Literature references about calculating the R factor in SMA-reinforced concrete frames are scarce. Alam et al. [14] obtained the overstrength and ductility factors through a static pushover analysis on concrete frames of 3, 6 and 8 storeys, reinforced with SMA bars in the plastic hinge zones. They obtained values for the overstrength factors of around 1.5, and about 2 for ductility, with minor variations depending on the design. In both cases, values were lower than those in the present study. The reason for this difference could lie in the number of bays, six in the referred study and only 1-2 in the present study, which limits plastic force redistribution and imposes the provision of more reinforcement in the design phase, which results in increased overstrength. Other factors could include different code provisions, building importance class, ductility class or different basic acceleration. This should draw our attention to the applicability of the results depending on the geographic location, geometry and importance of the building.

Other authors have studied the R factor in steel buildings with SMA bracings. For example, Ghassemieh et al. [49] obtained these factors through a dynamic nonlinear analysis done with different configurations of bracings, who obtained substantially mhigher R values. Buildings were designed with a preliminary R value of 9, but performance values up to 16 were obtained in the non-linear dynamic simulations. As in this study, both the overstrength factor and R factor reduced with frame height.

Table 14. Reduction factor R obtained for buildings 3S1B and 6S2B.

	Steel & NSC		SMA & NSC		Steel & HPC		SMA & HPC		Steel & UHPC		SMA & UHPC	
	3S1B	6S2B	3S1B	6S2B	3S1B	6S2B	3S1B	6S2B	3S1B	6S2B	3S1B	6S2B
Chi-Chi	7.14	6.90	5.33	4.44	8.12	9.59	7.22	9.18	7.75	10.07	9.88	11.91
Tabas	5.88	4.23	7.77	6.88	6.59	4.84	10.17	4.51	10.04	5.06	8.37	5.33
Kocaeli	7.21	4.30	12.26	4.96	6.62	4.50	15.86	5.00	7.72	5.25	16.10	5.24
Lomaprieta	8.22	3.02	13.96	6.46	6.85	2.94	12.36	2.59	5.59	5.07	4.59	3.32
L'Aquila	6.32	3.83	9.51	3.98	6.33	4.70	6.78	5.09	5.80	4.85	7.47	5.80
Average	*6.95*	*4.46*	*9.77*	*5.34*	*6.90*	*5.31*	*10.48*	*5.27*	*7.38*	*6.06*	*9.28*	*6.32*
C.V. (%)	*13.0*	*32.7*	*35.3*	*23.7*	*10.2*	*47.2*	*36.0*	*45.6*	*24.5*	*37.1*	*46.0*	*51.7*

7. Conclusions.

In this study, a comparative analysis of using new materials in the beam-column and column-foundation joints was made to improve the seismic behaviour of RC buildings. Two prototype typologies (3 and 6 heights), with plastic hinge zones built with six different material combinations, were designed for this purpose. A non-linear static pushover analysis and an incremental dynamic analysis (IDA) were carried out, in which simulations were made in the time domain of those buildings subjected to six different historical ground motions, and incrementally scaled according to the IDA technique. The following conclusions can be drawn from the analysis of the simulations:

- The concrete type in the joint, especially the lower stiffness of SMA, can significantly modify a building's dynamic characteristics, which must be taken into account when designing a building, as must the site's frequency spectrum.
- According to the definition of ductility in roof drift terms, using SMA can lower its value for conventional RC buildings. The use of UHPC allows loss of ductility to be recovered in the analysed low-rise buildings and to improve it in mid-rise ones.
- The largest drifts occur on the first floor in a most pronounced manner for SMA reinforcement due to the resistant mechanism generated at the ends of the first floor column. Using more rigid concrete is recommended, such as HPC or UHPC, because they help to control this phenomenon, and to avoid damage to non-structural elements.
- Designs with steel have lower drifts than those with SMA given their higher Young's modulus in relative terms; however, residual drifts are much lower in the designs that include SMA.
- The recentring property of SMA is more effective for 6-storey buildings as the damage that concentratesI on the first floor is lower because due the whole structure's stiffness is lower.

- The numerical study of the behaviour factor allows the values proposed by Eurocode 8 to be anticipated as being conservative, and this factor can be increased (and to, therefore, reduce the elastic stresses of the design) for the designs modified with new materials, which allows designs for smaller forces which, therefore, result in more economical designs, but with better seismic performance in residual drifts terms.

Finally, the study showed that using SMA combined with UHPC and a transition zone in the first floor columns presented much better performance in residual drifts terms by maintaining, or even improving, the ductility and resistance capacity in relation to the conventional solution. In this work, preliminary research was conducted to explore the potential application of the new materials (SMA and UHPC) in the MRF design. The numerical model has the following limitations: slippage between the steel or SMA bars and the mechanical coupler is not considered, perfect adherence between bars and any concrete type, critical zone length was set equal to 1.5-fold the depth for all the elements, beams and columns.

For future research works, a case-by-case study according to the building's location is proposed, for which it is convenient to use a large set of site ground motions. It is also mandatory to optimise the dimensions of the members along the height and length of SMA reinforcement, and to include SMA bars in the bond-slip behaviour joint. In this study, the topology of the modified zones was not analysed to determine the most efficient positions to minimise damage and to optimise the seismic behaviour because behthis is left for further research to do. Finally, it would be interesting to propose an expression for the plastic hinge length of the critical zones manufactured with UHPC and SMA bars to facilitate the design and to extend the application of such solutions.

8. Acknowledgements.

This article forms part of the research conducted at the Concrete Science and Technology Institute (ICITECH) of the Universitat Politècnica de València (UPV). This

work has been supported by the Spanish Ministry of Economy and Competitiveness through Project BIA2012-32645, and by the European Union through FEDER funds. The authors thank the Spanish Ministry of Education, Culture and Sport for Grant FPU13/06337.

References.

[1] Fardis MN. Seismic Design, Assessment and Retrofitting of Concrete Buildings. vol. 8. 2009. doi:10.1007/978-1-4020-9842-0.

[2] Pereiro-Barceló J, Bonet JL, Gómez-Portillo S, Castro-Bugallo C. Ductility of high-performance concrete and very-high-performance concrete elements with Ni-Ti reinforcements. Constr Build Mater 2018;175:531–51. doi:10.1016/j.conbuildmat.2018.04.172.

[3] Lagoudas DC. Shape Memory Alloys: Modeling and Engineering Applications. Springer; 2008. doi:10.1007/978-0-387-47685-8.

[4] Jani JM, Leary M, Subic A, Gibson MA. A review of shape memory alloy research, applications and opportunities. Mater Des 2014;56:1078–113. doi:10.1016/j.matdes.2013.11.084.

[5] McCormick J, DesRoches R, Fugazza D, Auricchio F. Seismic Vibration Control Using Superelastic Shape Memory Alloys. J Eng Mater Technol 2006;128:294. doi:10.1115/1.2203109.

[6] Saiidi S, Wang H. Exploratory study of seismic response of concrete columns with shape memory alloys reinforcement. ACI Struct J 2006;103:436–43.

[7] Youssef M a., Alam MS, Nehdi M. Experimental Investigation on the Seismic Behavior of Beam-Column Joints Reinforced with Superelastic Shape Memory Alloys. J Earthq Eng 2008;12:1205–22. doi:10.1080/13632460802003082.

[8] Abdulridha A, Palermo D, Foo S, Vecchio FJ. Behavior and modeling of superelastic shape memory alloy reinforced concrete beams. Eng Struct 2013;49:893–904. doi:10.1016/j.engstruct.2012.12.041.

[9] Shrestha B, Hao H. Performance-based seismic assessment of shape memory alloy reinforced bridge pier considering combined peak and residual deformations 2015.

[10] Zafar A, Andrawes B. Incremental dynamic analysis of concrete moment resisting frames reinforced with shape memory composite bars. Smart Mater Struct 2012;21:25013. doi:10.1088/0964-1726/21/2/025013.

[11] Zafar A, Andrawes B. Seismic behavior of SMA-FRP reinforced concrete frames under sequential seismic hazard. Eng Struct 2015;98:163–73. doi:10.1016/j.engstruct.2015.03.045.

[12] Alam MS, Youssef MA, Nehdi M. Analytical prediction of the seismic behaviour of superelastic shape memory alloy reinforced concrete elements. Eng Struct 2008;30:3399–411. doi:10.1016/j.engstruct.2008.05.025.

[13] Alam MS, Nehdi M, Youssef M. Seismic performance of concrete frame structures reinforced with superelastic shape memory alloys. Smart Struct Syst 2009;5:565–85.

[14] Alam MS, Moni M, Tesfamariam S. Seismic overstrength and ductility of concrete buildings reinforced with superelastic shape memory alloy rebar. Eng Struct 2012;34:8–20. doi:10.1016/j.engstruct.2011.08.030.

[15] Youssef MA, Elfeki MA. Seismic performance of concrete frames reinforced with

Superelastic Shape Memory Alloys. Smart Struct Syst 2012;9:313–33. doi:10.12989/sss.2012.9.4.313.

[16] Castro-Bugallo C. Análisis experimental de soportes de hormigón de altas prestaciones sometidos a compresión y carga lateral cíclica. Polytechnic University of Valencia, 2016.

[17] Takatsu H, Kimura H, Ishikawa Y. Experimental study of steel fiber-reinforced ultra-high strength concrete columns. 2nd Int. Congr. - FIB, Naples, Italy: 2006, p. 10.

[18] Voo YL, Poon WK, Foster SJ. Shear Strength of Steel Fiber-Reinforced Ultrahigh- Performance Concrete Beams without Stirrups. J Struct Eng 2010. doi:10.1061/(ASCE)ST.1943-541X.0000234.

[19] Zohrevand P, Mirmiran A. Cyclic Behavior of Hybrid Columns Made of Ultra High Performance Concrete and Fiber Reinforced Polymers. J Compos Constr 2012. doi:10.1061/(ASCE)CC.1943-5614.0000234.

[20] Popa M, Kiss Z, Tibea C, Bolca G, Tibea M, Constantinescu H. EXPERIMENTAL ANALYSIS AND NUMERICAL SIMULATION OF ULTRA-HIGH PERFORMANCE AND NORMAL CONCRETE COMPOUND COLUMNS. Bul Institutului Politeh Din Lasi Sect Constr Arhit 2013.

[21] Kamal MM, Safan MA, Etman ZA, Salama RA. Behavior and strength of beams cast with ultra high strength concrete containing different types of fibers. HBRC J 2014. doi:10.1016/j.hbrcj.2013.09.008.

[22] Maya LF, Zanuy C, Albajar L, Lopez C, Portabella J. Experimental assessment of connections for precast concrete frames using ultra high performance fibre reinforced concrete. Constr Build Mater 2013. doi:10.1016/j.conbuildmat.2013.07.002.

[23] Song G, Ma N, Li H-N. Applications of shape memory alloys in civil structures. Eng Struct 2006;28:1266–74. doi:10.1016/j.engstruct.2005.12.010.

[24] European Commitee for Standardization. Eurocode 8: Design of structures for earthquake resistance - Part 1 : General rules, seismic actions and rules for buildings. Eur Comm Stand 2004. doi:[Authority: The European Union per Regulation 305/2011, Directive 98/34/EC, Directive 2004/18/EC].

[25] Pereiro-Barceló J, Bonet JL, Cabañero-Escudero B, Martínez-Jaén B. Cyclic behavior of hybrid RC columns using High-Performance Fiber-Reinforced Concrete and Ni-Ti SMA bars in critical regions. Compos Struct 2019;212:207–19. doi:10.1016/j.compstruct.2019.01.029.

[26] Billah AHMM, Shahria Alam M. Plastic hinge length of shape memory alloy (SMA) reinforced concrete bridge pier. Eng Struct 2016;117:321–31. doi:10.1016/j.engstruct.2016.02.050.

[27] Paulay T, Priestley MJN. Seismic Design of Reinforced Concrete and Masonry Buildings. New York: John Willey & Sons, Inc.; 1992. doi:10.1016/0167-4730(93)90008-O.

[28] En1991-1-1:2002. Eurocode 1: Actions on structures - Part 1-1: General actions - Densities, self-weight, imposed loads for buildings. Eurocode 1, vol. 2, 2002. doi:10.1520/E2019-03R13.Copyright.

[29] McKenna F. OpenSees: A framework for earthquake engineering simulation. Comput Sci Eng 2011;13:58–66. doi:10.1109/MCSE.2011.66.

[30] Mazzoni, S.; McKenna, F.; Scott, M. H.; Fenves GL. Open System for Earthquake Engineering Simulation (OpenSees). OpenSees Command Language Manual. Berkeley, CA: Pacific Earthquake Engineering Research Center, University of California; 2006.

[31] Alam MS, Youssef M a., Nehdi ML. Exploratory investigation on mechanical

anchors for connecting SMA bars to steel or FRP bars. Mater Struct 2010;43:91–107. doi:10.1617/s11527-010-9601-0.

[32] Haber ZB, Saiidi MS, Sanders DH. Seismic performance of precast columns with mechanically spliced column-footing connections. ACI Struct J 2014;111:639–50. doi:10.14359/51686624.

[33] Nakashoji BA. Seismic Performance of Square Nickel-Titanium Reinforced ECC Columns with Headed Couplers. University of Nevada, Reno, 2014.

[34] Billah AHM, Alam SM. Seismic performance of concrete columns reinforced with hybrid shape memory alloy (SMA) and fiber reinforced polymer (FRP) bars. Constr Build Mater 2012;28:730–42. doi:10.1016/j.conbuildmat.2011.10.020.

[35] Lagoudas DC, Bo Z. Thermomechanical modeling of polycrystalline SMAs under cyclic loading, Part II: Material characterization and experimental results for a stable transformation cycle. Int J Eng Sci 1999;37:1141–73. doi:10.1016/S0020-7225(98)00114-1.

[36] Shaw JA, Churchill CB, Iadicola MA. Tips and tricks for characterizing shape memory alloy wire: Part 1-differential scanning calorimetry and basic phenomena. Exp Tech 2008;32:55–62. doi:10.1111/j.1747-1567.2008.00410.x.

[37] Fedération Internationale du Béton; Comité euro-international du béton; Fédération international de la précontrainte. fib Model Code for Concrete Structures 2010. Berlin: Ernst & Sohn; 2013. doi:10.1002/9783433604090.

[38] Mander JB, Priestley MJN, Park R. Theoretical stress-strain model for confined concrete. J Struct Eng 1988. doi:10.1061/(ASCE)0733-9445(1988)114:8(1804).

[39] Campione G. The effects of fibers on the confinement models for concrete columns. Can J Civ Eng 2002. doi:10.1139/l02-066.

[40] Aslani F, Nejadi S. Cyclic constitutive model for high-strength concrete confined by ultra-high-strength and normal-strength transverse reinforcements. Aust J Struct Eng 2012.

[41] Aslani F, Jowkarmeimandi R. Stress-strain model for concrete under cyclic loading Stress–strain model for concrete under cyclic loading. Mag Concr Res 2012. doi:10.1680/macr.11.00120.

[42] Saiidi MS, O'Brien M, Mahmoud SZ. Cyclic response of concrete bridge columns using superelastic nitinol and bendable concrete. ACI Struct J 2009. doi:10.14359/56285.

[43] ATC. Quantification of building seismic performance factors. 2009. doi:10.1016/j.compstruc.2009.08.001.

[44] Code UB. Uniform building code. 1997. doi:10.14694/EdBook_AM.2014.34.e461.

[45] American Society of Civil Engineers (ASCE). Minimum design loads for buildings and other structures (ASCE/SEI 7-05). 2006. doi:10.1061/9780784412916.

[46] Chopra AK. Dynamics of structures : theory and applications to earthquake engineering. Pearson Educ 2007. doi:10.1002/9781118599792.

[47] Gerami M, Mashayekhi AH, Siahpolo N. Computation of R Factor for Steel Moment Frames by Using Conventional and Adaptive Pushover Methods. Arab J Sci Eng 2017;42:1025–37. doi:10.1007/s13369-016-2257-5.

[48] Zafar A. Response modification factor of reinforced concrete moment resisting frames in developing countries. University of Illinois at Urbana-Champaign, 2009.

[49] Ghassemieh M, Kargarmoakhar R. Response modification factor of steel frames utilizing shape memory alloys. J Intell Mater Syst Struct 2013;24:1213–25. doi:10.1177/1045389X12471869.